8-14-2014 12:00 AM

Numerical Analysis of Two Phase Flow and Heat Transfer in Condensers

Pooya Mirzabeygi
The University of Western Ontario

Supervisor
Prof. Chao Zhang
The University of Western Ontario

NUMERICAL ANALYSIS OF TWO PHASE FLOW AND HEAT TRANSFER IN
CONDENSERS

(Thesis format: Integrated Article)

by

Pooya Mirzabeygi

Graduate Program in Mechanical and Materials Engineering

A thesis submitted in partial fulfillment
of the requirements for the degree of
Masters of Engineering Science

The School of Graduate and Postdoctoral Studies
The University of Western Ontario
London, Ontario, Canada

Abstract

Steam surface condensers are commonly used in the power generation industry and their performance significantly affects the efficiency of the power plant. Therefore, it is vital to acquire a better understanding of the complex phenomena occurring inside condensers. A general three-dimensional numerical model is developed in this study to simulate the two-phase flow and heat transfer inside full-scale industrial condensers with irregular tube bundle shapes. The Eulerian-Eulerian two-phase model is selected to simulate gas and liquid flows and the interaction between them. A porous media approach is adopted to model the presence of large number of tubes in the condenser. The effect of the turbulence on the primary phase is accounted for by solving the transport equations for turbulent kinetic energy and dissipation rate. Various types of turbulence models are evaluated to select the best model for the condenser analysis. Also, the modified k-ε and RNG k-ε models are proposed to model the flow and heat transfer in condensers by adding the corresponding terms to the transport equations of the turbulence model to account for the effects of the tube bundle and condensate droplets on the primary phase turbulence, momentum and heat transfer. The proposed model provides excellent match with the experimental data and a significant improvement over the previous models. Furthermore, the proposed numerical model is coupled with a novel swarm intelligence multi-objective optimization algorithm to evaluate the performance of the new design candidates and introduce a set of condenser designs based on various input parameters and objective functions.

Keywords

Co-Authorship Statement

There are three submitted journal papers included in this thesis. All papers are written by Pooya Mirzabeygi and modified under the supervision of Prof. Chao Zhang.

Acknowledgments

Table of Contents

List of Tables

List of Figures

Nomenclature

a, b	constants	g	gravitational acceleration
A	heat transfer area	h	heat transfer coefficient
$C_{1\varepsilon}$, $C_{2\varepsilon}$	constants in turbulence transport equations	J	diffusion flux of the air in the vapor
$C_{\varepsilon b}$	coefficient	K	swarm size
C_{fx}, C_{fy}	interphase friction coefficient	k	turbulent kinetic energy
C_{phase}	interphase exchange coefficient	L	latent heat of condensation
C_P	Specific heat	$\dot{m}$	condensation rate
D	Diffusivity of air in steam	n	inundation index
f	friction factor due to tube bundle	N	dimensional size of design space
f_d	friction factor due to interphase friction	Nu	Nusselt number
f_R	darcy friction factor	p	Pressure
F	Particles' fitness	P	particles' individual memory position vector at each time step
G_k	generation of turbulent kinetic energy	P_t	tube pitch
G	swarm global memory position vector	P^*	position vector for guidance of particles in the swarm

Pr	Prandtl number	V_L	volume of the computational cell
R	thermal resistance	VP	Particle velocity vector at in the swarm
Ra	territory radius at each time step	W	inertia weight
Rb	source term due to tube bundle	Wb	source term due to interphase friction
RG	source term for RNG k-ε	X	Particle position vector in the swarm
Re	Reynolds number	Y	dissipation of k or ε
S	general source term	**Greek Symbols**	
S_{mass}	continuity source term	α	porosity
S_{mom}	momentum source term	β	volume fraction
S_{diff}	species transport source term	Γ	effective diffusivity
t	optimization iteration (time step)	γ_c	condensation rate in the control volume
T	temperature	γ_{tot}	condensate leaving the control volume
U	velocity magnitude	δ	polynomial probability distribution
u	x-velocity	ε	turbulent kinetic energy dissipation rate
V	velocity vector	η	polynomial distribution index
v	y-velocity	θ	air mass fraction

λ	thermal conductivity	d	droplet
μ	laminar viscosity	eff	effective
ξ	pressure loss coefficient	g	gas-mixture
ρ	density	id	inside diameter
σ	turbulent Prandtl number	k	parameter for turbulent kinetic energy
τ	time scale	l	liquid
$\bar{\bar{\tau}}$	stress tenser	p	particle
ϕ_1, ϕ_2, ϕ_3	constants in the optimization algorithm	od	outside diameter
χ	constriction coefficient	ow	tube outside wall
ω	specific dissipation rate	rel	relative

Subscripts

		s	steam
a	non-condensable-gas (air)	tw	tube wall
c	liquid condensate	ε	parameter for turbulent kinetic energy dissipation rate
ci	condensate film interphase		**Superscript**
cw	coolant water	t	optimization iteration (time step)

spins the steam turbine to generate power. After it passes through the turbine, the steam is condensed in a condenser. A simplified diagram of a thermal power station is given in Figure 1-2. Figure 1-3 shows the schematic view of an industrial steam surface condenser [1].
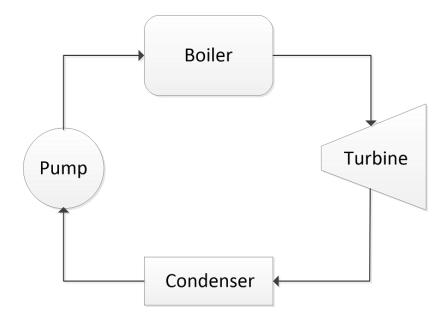
Figure 1-2: Simplified schematic diagram of a thermal power station
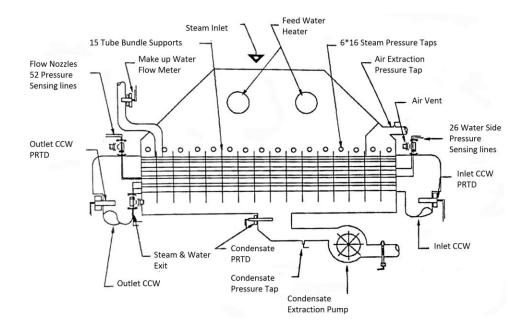
Figure 1-3: Schematic view of an industrial steam surface condenser [1]

There are two independent flow regions in this type of condensers that are separated by the tube walls: shell-side and tube-side. Steam is flowing in the shell-side around the tubes and condenses in contact with their cold surfaces. There are two mechanisms of condensation in this case: drop-wise and film-wise condensation. In drop-wise condensation, the droplets of liquid forms around the tube and they remain separated until they are carried away by gravity or shear. On the contrary, in the film-wise condensation, the condensate totally wets the surface and the cold surface is only exposed to the liquid film. For most of the industrial applications, film-wise condensation mechanism is the dominant mode, especially for the cases with high condensate flow rate. Then, the condensate film formed in this process falls due to the gravity and vapor shear on the lower tubes and finally exits the domain to be reused in steam generator or boiler in the next cycle. This increase in the amount of condensate flow on the lower tubes is called inundation. The inundation phenomenon, that significantly deteriorates the heat transfer rate on the tubes involved, occurs in three different modes or regimes: droplet mode, column mode and sheet mode.

Also, steam is not the only constituent of the mixture that flows in the shell-side of the condenser. No matter how perfect the design of the power plant is, there still will be some improper sealing or leaks in the system that non-condensable gases, mainly air, can get into the system. It is well known that non-condensable gases play a significant role in heat transfer reduction around cold surfaces; even small amount of non-condensable gases will form a thermally insulating blanket around tubes which inhibits the heat and mass transfer from the vapor-air mixture to the liquid film. Moreover, the existence of non-condensable gases in the vapor-gas mixture reduces the partial pressure of the steam that will in turn decrease the steam saturation temperature and further deteriorates the heat transfer. Therefore, there is a vent system in most of the condensers today that extracts the non-condensable gases accumulated in the system. Of course, some of the steam will also leave the domain alongside the non-condensable gases.

Moreover, the vapor-gas mixture that flows in the shell-side is turbulent as it exits the final stages of the turbine with high velocity. Therefore, it is extremely important to consider the turbulence effect in the gas phase and the factors that influence it. First, the

existence of large number of tubes in the condenser enhances the turbulence in the vapor-air mixture. Also, the liquid phase droplets formed in the condensation process not only affects the flow of the vapor-gas mixture through interphase friction, but also they contribute to the turbulence augmentation in the primary phase.

Finally, the cooling water flows in the tubes perpendicular to the main flow direction of the gas-phase, while the two fluid streams never come to contact with each other. The cooling water flow inside the tubes is an example of a turbulent forced convection inside cylindrical tubes, which is fully understood and analyzed in the literature. However, the heat transfer between the two streams is far more complex, and various thermal resistances need to be considered. These thermal resistances, which include the resistances due to the temperature gradient in the cooling water side, tube wall, condensate film and non-condensable gases, determine and restrict the heat transfer between shell and tube-side flows. Among them, the thermal resistances due to the condensate film and non-condensable gases are very difficult to model. The former is greatly affected by the combined effects of the gravity, vapor shear and condensate inundation. The latter requires the knowledge of the air mass concentration at the gas-liquid interface.

1.2   Literature review

Studies on shell-and-tube heat exchangers and in particular steam surface condensers have been carried out by many researchers as they are an integral part of a power plant and even a small improvement in their efficiency or performance can lead to a significant reduction in operational costs of the power generation unit and the electricity price. The conventional way to improve condenser design was through trial and error approach based on the designer's experience and experimental data [2-5]. However, without an in-depth understanding of flow and heat transfer inside the condensers it is difficult if not impossible to achieve this goal. Moreover, performing experimental analysis on each and every design candidate is extremely costly and time-consuming [6]. Not to mention the difficulties the experimentalists face to obtain the detailed measurement of turbulent flow in full-scale industrial condensers that are usually several meters in size and consist of thousands of tubes. Thus, the numerical analysis is a viable option that can provide

detailed information on the flow and heat transfer inside the condensers and is also considerably less expensive than the experimental method.

Several numerical models have been proposed for the simulation of the flow and heat transfer in condensers and they can be classified into two categories.

First one is to solve the detailed flow and heat transfer around each and every tube in the condenser. This method is practically impossible to be applied on the analysis of large industrial condensers since industrial condensers usually have thousands of tubes. However, in recent years, the modeling of condensation around cold surfaces with simple geometry (e.g. flat plate) using CFD methods has gained more and more popularity. Although these methods are still at the preliminary stages of development, it is important to consider them as the future methods in this type of analysis. Benelmir et al. [7] modeled the water vapor condensation with non-condensable gases in a plate heat exchanger. Guo et al. [8] proposed a volume-of-fluid level set (VOSET) method to simulate film boiling problem. Riva and Col [9] performed three-dimensionality analysis of film-condensation inside a mini-channel using VOF model. Liu et al. [10] developed a computational model to predict the film condensation heat transfer between vertical parallel plates using VOF model. Dahikar et al. [11, 12] studied the co-current downward steam condensation in a vertical pipe using VOF method. Lejon [13] performed a comparative analysis on the condensation modeling capabilities of commercial software; the two-dimensional flat plate was used as the test case. Later, Sun et al. [14] proposed a new VOF condensation modeling suitable for the case that both unsaturated phase and saturated phase are present. Dehbi et al. [15] proposed a numerical model for condensation modeling in presence of non-condensable gases in ANSYS FLUENT which neglects the thermal resistance of the liquid film. Most of these researches are devoted to the analysis of film condensation on a flat surface and the analysis of the phenomenon is yet to be done for cylindrical tubes, and it is important to note that this approach is still far away from being tested on real life industrial condensers.

The second method, however, does not require solving the detailed flow and temperature fields around each tube. The tube bundle region is regarded as porous media which

restricts the main flow by distributed resistance. Patankar and Spalding [16] were pioneers in this field as they introduced the porous media concept to account for the tube bundle's drag force, and consequently, they reduced the computational time significantly as their numerical procedure does not require the detailed analysis around each tube. Many models adopted this approach in their simulations and it proves to match experimental data with a reasonable accuracy [1, 17-36]; these models can be classified into two main categories: single-phase and two-phase models.

Single-phase models neglect the effect of the second phase and assume that the condensate disappears from the domain as it is formed. Davidson and Rowe [17] solved the single-phase equations and used Berman and Fuks correlation to account for the effect of non-condensable gases. Al-Sanea et al. [18], Malin [23], Roy et al. [24], Prieto et al. [25], Ormiston et al. [26, 27], and Zhang et al. [34] were among the first researchers who performed this type of analysis; they neglected the inundation and the interphase effect on the fluid flow and used a single-phase model in their simulations. Zhang and Zhang [36] studied the sensitivity of condensation heat transfer coefficient using a single-phase model. Zhang [16] studied the effects on the heat transfer rate due to the inundation, inlet air mass fractions, and cooling water flow rates. The single-phase model was used in this study. He et al. [2] performed a three-dimensional single-phase analysis using a modified k-ε model on shell-and-tube heat exchangers. Nedelkovski et al. [37] developed a finite element method to three-dimensional single-phase equations for the condenser; they considered the effect of non-condensable gases. Later, Rusowicz [38] performed the single-phase two-dimensional steady state model on 50 MW plant condenser and reported satisfactory results. Zeng et al. [4] solved the single-phase mixture equation for steam and non-condensable gases in addition to RNG k-ε model to study different tube arrangements for 300 MW power plant condenser.

Two-phase models regard both gas-mixture and liquid as continuous and interpenetrating fluids, and the interaction between the phases are modeled. The first model was developed by Al-Sanea et al. [19], in which they included the interphase effect in their two-phase model. Rabas and Kassem [20] studied the effect of condensate inundation effect and neglected vapor shear effect on convective heat transfer. McNaught and

Cotchin [21] implemented a new correlation to account for the effects of inundation. Bush et al. [22] predicted flow and heat transfer in an experimental condenser using a two-phase model. Moreover, Zhang and Bokil [32] included the interphase effect and used a two-phase model to simulate a condenser. Hu and Zhang [28] developed a modified k-ε turbulence model for two-phase flow in condensers and later assessed the effects of different closure correlation on the numerical simulations [29] and proposed a new correlation for the effect of inundation on convective heat transfer [30].

One of the critical challenges that numerical methods face to model the flow inside condensers is how to deal with turbulence effects. Therefore, it is important to look at the literature from this perspective. In most of the earlier researches, the effect of turbulence was neglected [3, 17, 24, 25, 32, 38]. Later, constant viscosity ratio or a simple algebraic equation were considered to account for the turbulence [22, 23, 39]. Gomez et al. [40] used a length scale (proportional to the clearance between the tubes) and a velocity fluctuation to modify the effective viscosity. A more recent approach is to solve the turbulence equations for shell-side flow using different turbulence models to model the turbulent viscosity. Sha et al. [41] proposed a one-equation turbulence model based on transport equation for turbulent kinetic energy to account for tube-bundle resistance. Later, several authors [2, 6, 28, 42] solved the k-ε equations to model the turbulent viscosity in the vapor-air mixture, and finally, Zeng et al. [4] implemented the RNG k-e turbulence model without any additional terms in their numerical solution.

Nonetheless, none of the researchers used their proposed numerical algorithm to develop a procedure to improve the condenser performance. The research works on the heat exchangers design optimization are summarized here. First, Selbas et al. [43] used a logarithmic mean temperature difference (LMTD) method and genetic optimization method to find the optimal design of the shell-and-tube heat exchangers. Ponce-Ortega et al. [44] used Bell-Delaware [45] method in combination with genetic algorithm to find the optimized design of a shell-and-tube condenser. Later, Fesanghary et al. [46] used the global sensitivity analysis (GSA) and harmony search algorithm (HSA) for design optimization of shell and tube heat exchangers from the economic viewpoint. They used Bell-Delaware method to obtain the average shell side heat transfer coefficient. Patel and

Rao [47] solved a cost minimization using Particle Swarm Optimization (PSO) technique and LMTD method. Zeng et al. [4] studied three conventional tube configurations and proposed a new tube configuration based on the analysis. However, CFD methods provide more detailed and accurate results in comparison with the simplified models like LMTD, and there is a need of developing a numerical procedure to couple the CFD models with an optimization technique to obtain improved condenser designs.

1.3   Thesis Objectives

The main objectives of this thesis are given as follows:

1.   To improve the numerical modeling for the two-phase flow and heat transfer in condensers with the focus given to develop improved turbulence models.
2.   To provide a comprehensive three-dimensional CFD model based on porous media approach for the numerical analysis of large industrial condensers with irregular tube bundle shapes.
3.   To develop a new optimization algorithm for condenser designs by coupling the proposed CFD model with a novel multi-objective optimization algorithm.

1.4   Thesis Outline

This thesis is organized as follows:

The first chapter is devoted to provide an introduction for this research. The background information, literature review, thesis objectives and outline are given in this chapter.

The turbulence modeling in condensers is presented in Chapter two. The comparative analysis of different turbulence models is conducted and the best turbulence model, based on comparison with experimental data, is selected. Moreover, an improved modified k-ε model and a modified RNG k-ε turbulence model are proposed that include the effects of the tube bundle and dispersed liquid phase on the gas phase turbulence.

In chapter three, a comprehensive three-dimensional Eulerian multiphase numerical model is presented to solve the fluid flow and heat transfer in both the experimental and full-scale industrial condensers. Both quasi-three-dimensional and three-dimensional

approaches are used. The numerical results are compared with the experimental data available in the literature and the comparisons show that the numerical method is capable of accurately modeling the flow and heat transfer in both the small-scale experimental condenser and the large-scale industrial condenser with irregular tube bundle shapes.

Next, in chapter four, a systematic procedure to optimize the condenser design is proposed by coupling the CFD model developed in the previous chapters with a multi-objective optimization algorithm. Multi-objective Territorial Particle Swarm Optimization (MOTPSO) method is used to obtain a set of optimized designs with respect to various objective functions considered.

Finally, a conclusion and recommendation for future work are provided in chapter five.

References

[1]   C. Zhang, "Numerical modeling using a quasi-three-dimensional procedure for large power plant condensers," *Journal of heat transfer,* vol. 116, pp. 180-188, 1994.

[2]   Y. He, W. Tao, B. Deng, X. Li, and Y. Wu, "Numerical simulation and experimental study of flow and heat transfer characteristics of shell side fluid in shell-and-tube heat exchangers," in *Proceedings of Fifth International Conference on Enhanced, Compact and Ultra-Compact Heat Exchangers: Science, Engineering and Technology, Hoboken, NJ, USA*, 2005, pp. 29-42.

[3]   I. S. Ramón and M. P. González, "Numerical study of the performance of a church window tube bundle condenser," *International journal of thermal sciences,* vol. 40, pp. 195-204, 2001.

[4]   H. Zeng, J. a. Meng, and Z. Li, "Numerical study of a power plant condenser tube arrangement," *Applied Thermal Engineering,* vol. 40, pp. 294-303, 2012.

[5]   S. Kakac, H. Liu, and A. Pramuanjaroenkij, *Heat exchangers: selection, rating, and thermal design*: CRC press, 2012.

[6]   M. Prithiviraj and M. J. Andrews, "Three dimensional numerical simulation of shell-and-tube heat exchangers. Part I: foundation and fluid mechanics," *Numerical Heat Transfer, Part A: Applications,* vol. 33, pp. 799-816, 1998/06/01 1998.

[7]   R. Benelmir, S. Mokraoui, and A. Souayed, "Numerical analysis of filmwise condensation in a plate fin-and-tube heat exchanger in presence of non-condensable gas," *Heat and mass transfer,* vol. 45, pp. 1561-1573, 2009.

[8]   D. Guo, D. Sun, Z. Li, and W. Tao, "Phase change heat transfer simulation for boiling bubbles arising from a vapor film by the VOSET method," *Numerical Heat Transfer, Part A: Applications,* vol. 59, pp. 857-881, 2011.

[9]   E. Da Riva and D. Del Col, "Numerical simulation of laminar liquid film condensation in a horizontal circular minichannel," *Journal of Heat Transfer,* vol. 134, p. 051019, 2012.

[10]   Z. Liu, B. Sunden, and J. Yuan, "VOF modeling and analysis of filmwise condensation between vertical parallel plates," *Heat Transfer Research,* vol. 43, 2012.

[11]   S. K. Dahikar, A. A. Ganguli, M. S. Gandhi, J. B. Joshi, and P. K. Vijayan, "Heat transfer and flow pattern in co-current downward steam condensation in vertical pipes-I: CFD simulation and experimental measurements," *The Canadian Journal of Chemical Engineering,* vol. 91, pp. 959-973, 2013.

[12]   A. A. Ganguli, S. K. Dahikar, M. S. Gandhi, J. B. Joshi, and P. K. Vijayan, "Heat transfer and flow pattern in co-current downward steam condensation in vertical pipes-II: Comparison with published work," *The Canadian Journal of Chemical Engineering,* vol. 91, pp. 974-991, 2013.

[13]   M. Lejon, "Wall Condensation Modelling in Convective Flow," *KTH, Heat and Power Technology*, 2013.

[14]   D.-L. Sun, J.-L. Xu, and L. Wang, "Development of a vapor–liquid phase change model for volume-of-fluid method in FLUENT," *International Communications in Heat and Mass Transfer,* vol. 39, pp. 1101-1106, 2012.

[15]   A. Dehbi, F. Janasz, and B. Bell, "Prediction of steam condensation in the presence of noncondensable gases using a CFD-based approach," *Nuclear Engineering and Design,* vol. 258, pp. 199-210, 2013.

[16]   S. Patankar and D. Spalding, "Heat exchanger design theory source book," *Scripta Book Co., Washington, DC,* pp. 155-176, 1974.

[17]   B. Davidson and M. Rowe, "Simulation of power plant condenser performance by computational methods: an overview," *Power Condenser Heat Transfer Technology,* pp. 17-49, 1981.

[18]   S. Al-Sanea, N. Rhodes, D. Tatchell, and T. Wilkinson, "A computer model for detailed calculation of the flow in power station condensers," in *Condensers: theory and practice. Symposium*, 1983, pp. 70-88.

[19]   S. Al-Sanea, N. Rhodes, and T. Wilkinson, "Mathematical modelling of two-phase condenser flows," in *Proceedings of the BHRA 2nd International Conference on Multi-Phase Flow, London*, 1985, pp. 169-182.

[20]   T. Rabas and A. Kassem, "The Effect of Equal Shellside Pressure Drops on the Thermal Performance of Single-Pass,'X'-Shell, Steam Condensers," in *23rd ASME-AIChE National Heat Transfer Conference, Denver, Colorado*, 1985.

[21]   J. McNaught and C. Cotchin, "Heat transfer and pressure drop in a shell and tube condenser with plain and low-fin tube bundles," *Chemical engineering research & design,* vol. 67, pp. 127-133, 1989.

[22]   A. Bush, G. Marshall, and T. Wilkinson, "The prediction of steam condensation using a three component solution algorithm," in *Proceedings of the Second International Symposium on Condensers and Condensation, University of Bath, UK*, 1990, pp. 223-234.

[23]   M. R. Malin, "Modelling flow in an experimental marine condenser," *International Communications in Heat and Mass Transfer,* vol. 24, pp. 597-608, 1997.

[24]   R. Roy, V. Gokhale, and M. Ratisher, "A computational model of a power plant steam condenser," *Journal of energy resources technology,* vol. 123, pp. 81-91, 2001.

[25]   M. Prieto, I. Suarez, and E. Montanes, "Analysis of the thermal performance of a church window steam condenser for different operational conditions using three models," *Applied thermal engineering,* vol. 23, pp. 163-178, 2003.

[26]   S. Ormiston, G. Raithby, and L. Carlucci, "Numerical modeling of power station steam condensers—Part 1: Convergence behavior of a finite-volume model," *Numerical Heat Transfer,* vol. 27, pp. 81-102, 1995.

[27]   S. Ormiston, G. Raithby, and L. Carlucci, "Numerical modeling of power station steam condensers—Part 2: Improvement of solution behavior," *Numerical Heat Transfer,* vol. 27, pp. 103-125, 1995.

[28]   H. G. Hu and C. Zhang, "A modified k–ε turbulence model for the simulation of two-phase flow and heat transfer in condensers," *International Journal of Heat and Mass Transfer,* vol. 50, pp. 1641-1648, 2007.

[29]   H. G. Hu and C. Zhang, "Evaluations of closure correlations for the simulation of two-phase flows in condensers," *Heat Transfer Engineering,* vol. 30, pp. 437-451, 2009.

[30]   H. G. Hu and C. Zhang, "A new inundation correlation for the prediction of heat transfer in steam condensers," *Numerical Heat Transfer, Part A: Applications,* vol. 54, pp. 34-46, 2008.

[31]   C. Zhang, "Local and overall condensation heat transfer behavior in horizontal tube bundles," *Heat transfer engineering,* vol. 17, pp. 9-30, 1996.

[32]   C. Zhang and A. Bokil, "A quasi-three-dimensional approach to simulate the two-phase fluid flow and heat transfer in condensers," *International journal of heat and mass transfer,* vol. 40, pp. 3537-3546, 1997.

[33]   C. Zhang, A. Sousa, and J. Venart, "The numerical and experimental study of a power plant condenser," *Journal of heat transfer,* vol. 115, pp. 435-445, 1993.

[34]   C. Zhang, A. Sousa, and J. Venart, "Numerical simulation of different types of steam surface condensers," *Journal of Energy Resources Technology,* vol. 113, pp. 63-70, 1991.

[35]   C. Zhang and Y. Zhang, "A quasi-three-dimensional approach to predict the performance of steam surface condensers," *Journal of energy resources technology,* vol. 115, pp. 213-220, 1993.

[36]   C. Zhang and Y. Zhang, "Sensitivity analysis of heat transfer coefficient correlations on the predictions of steam surface condensers," *Heat transfer engineering,* vol. 15, pp. 54-63, 1994.

[37]   I. Nedelkovski, I. Vilos, and T. Geramitcioski, "Finite element solution of Navier-Stokes equations for steam flow and heat transfer," *Momentum,* vol. 1000, p. 1, 2005.

[38]   A. Rusowicz, "The numerical modeling and measurements for power plant condenser," 2009.

[39]   S. B. Beale, "A Simple, Effective Viscosity Formulation for Turbulent Flow and Heat Transfer in Compact Heat Exchangers," *Heat Transfer Engineering,* vol. 33, pp. 4-11, 2012.

[40]   A. Gómez, N. Fueyo, and L. I. Díez, "Modelling and simulation of fluid flow and heat transfer in the convective zone of a power-generation boiler," *Applied Thermal Engineering,* vol. 28, pp. 532-546, 2008.

[41]   W. Sha, T. Kao, S. Cho, and C. Yang, "Multidimensional numerical modeling of heat exchangers," *Journal of Heat Transfer,* vol. 104, pp. 417-425, 1982.

[42]   Y. You, A. Fan, S. Huang, and W. Liu, "Numerical modeling and experimental validation of heat transfer and flow resistance on the shell side of a shell-and-tube heat exchanger with flower baffles," *International Journal of Heat and Mass Transfer,* vol. 55, pp. 7561-7569, 2012.

[43]   R. Selbaş, Ö. Kızılkan, and M. Reppich, "A new design approach for shell-and-tube heat exchangers using genetic algorithms from economic point of view,"

Chemical Engineering and Processing: Process Intensification, vol. 45, pp. 268-275, 2006.

[44]   J. M. Ponce-Ortega, M. Serna-González, and A. Jiménez-Gutiérrez, "Use of genetic algorithms for the optimal design of shell-and-tube heat exchangers," *Applied Thermal Engineering,* vol. 29, pp. 203-209, 2009.

[45]   K. J. Bell, *Delaware method for shell-side design*, 1988.

[46]   M. Fesanghary, E. Damangir, and I. Soleimani, "Design optimization of shell and tube heat exchangers using global sensitivity analysis and harmony search algorithm," *Applied Thermal Engineering,* vol. 29, pp. 1026-1031, 2009.

[47]   V. K. Patel and R. V. Rao, "Design optimization of shell-and-tube heat exchanger using particle swarm optimization technique," *Applied Thermal Engineering,* vol. 30, pp. 1417-1425, 2010.

Chapter 2

2 Turbulence modeling for two-phase flow and heat transfer in condensers

2.1 Introduction

Heat transfer between two fluids at different temperatures is vital for most industrial processes, and heat exchangers are the devices that specifically designed for this purpose. Heat exchangers are widely used in a variety of applications, such as power production, petroleum refineries, chemical plants, food industries, air conditioning, refrigeration, sewage treatment etc. [1]. Among different types of heat exchangers, shell and tube heat exchangers are the most widely used (37% of total heat exchanger market) because of their simple manufacturing and adaptability to different ranges of operating conditions, pressures, and temperatures [2]. A shell and tube heat exchanger consists of a tube bundle mounted inside the shell. One fluid flows over the tubes (shell side) and the other fluid flows through the tubes, and heat transfer occurs between these two streams of fluids. The heat exchanger can operate in a single phase mode to heat up or cool down fluids or it can operate in a two-phase mode as an evaporator or condenser.

The focus of this study is on steam surface condenser which is a type of shell and tube heat exchanger commonly used in power plants to condense the exhaust steam from the turbine to liquid water in order to complete the thermal cycle. In this type of condensers, coolant water flows through the tube bundles to extract heat from the oncoming steam in the shell side. In the shell-side, the mixture of the steam and non-condensable gases flows around the tubes and the liquid condensate occurs. The liquid then falls down due to the gravity and exits the condenser at the bottom.

Many academic and industrial researches have devoted to improve the design of shell and tube heat exchangers in order to increase the thermal efficiency and reduce the energy consumptions. However, it is impossible to develop a reliable and efficient design without a detailed knowledge of the flow field and heat transfer in the heat exchangers. This knowledge can be obtained through numerical or experimental analysis. However,

experimental analysis is usually time-consuming and expensive; besides, it is difficult, if not impossible, to perform full scale measurements in an industrial condenser [3]. Moreover, with the introduction of new generation of computational resources that reduces the cost and time of the analysis, numerical models are getting more and more attention from researchers to provide accurate information on the flow and heat transfer in industrial applications. Therefore, a reliable, robust numerical model can be used as an alternative tool to provide further understanding into what is happening in a full scale industrial condenser.

Industrial condensers usually contain large number of tubes, and it is therefore practically impossible to solve the detailed fluid flow and heat transfer around each and every tube in the condenser. To solve this problem Patankar and Spalding [4] proposed a method to consider the pressure drop due to presence of tube bundles using porous media analogy. In this method, each computational cell may contain several tubes, and the effect of these tubes is accounted for by using a distributed resistance against the gross motion of the fluid. Many researchers adopted this approach due to its simplicity, easy implementation and robustness in solving large–scale industrial processes [3, 5-8].

Moreover, accounting for the presence of the tube bundle as a distributed resistance inhibiting the motion of shell side flow is not the only challenge in the road to develop a comprehensive numerical model that can accurately solve the flow field and heat transfer process in an industrial condenser. Other challenges are mostly due to the presence of turbulence in both vapor and condensate phases, large number of tubes, presence of non-condensable gases, three dimensionality effects due to the presence of coolant flow in the tubes, condensate inundation etc. Resolving all these complexities to the smallest details is currently not feasible due to limited computational resources. Among these difficulties, turbulence modeling is known to be the most challenging task mainly because there is not a universal turbulence model for multiphase flows that can accurately include the effects of gas-liquid interaction and tube bundles.

Numerical studies of condensers have been conducted by several researchers and different techniques have been proposed to deal with turbulence flows in condensers. In

most of the earlier researches, the effect of turbulence was neglected [9-14]. Later, a constant viscosity ratio or a simple algebraic equation was used to account for the turbulence [15-17]. Gomez et al. [18] used a length scale (proportional to the clearance between the tubes) and a velocity fluctuation to calculate the effective viscosity. A more recent approach is to solve the turbulence equations for the shell-side flow using different turbulence models to model the turbulent viscosity. Sha et al. [19] proposed a one-equation turbulence model based on transport equation for turbulent kinetic energy to account for tube-bundle resistance. Later, several researchers [3, 20-22] solved the k-ε equations to model the turbulent viscosity in the vapor-air mixture, and finally, Zeng et al. [23] implemented the RNG k-ε turbulence model in their numerical solution without considering the effects of tube bundles and two-phase interactions on the turbulence.

However, there has never been a research on comparative analysis of different turbulence models to study the effectiveness of the choice of turbulence models in the simulation of the fluid flow and heat transfer in condensers. Variations of k-ε models, Realizable k-ε [24] and RNG k-ε [25], and also other two equation models such as k-ω [26] and its modification, k-ω Shear Stress Transport (SST) [27], are known to perform better than the standard k-ε model especially at low-Reynolds number regions. The first objective of this chapter is to compare various turbulence models available for the simulation the complex fluid flow and heat transfer in a condenser.

The detailed analysis of the fluid flow and temperature distribution around each tube in a condenser is not computationally feasible due to large number of tubes in most industrial condensers. So, a porous media approach is often adopted to account for the presence of the tube bundle. Tube bundle is not only a source of resistance to the flow; it also enhances the dissipation and production of the turbulent kinetic energy and should be considered as source terms in turbulence equations. In some earlier studies, the dot product of the resistance and velocity vector was simply added to the turbulent kinetic energy equation (k) [3, 20-22] to take the presence of tube bundles into account. However, new models are now available due to the recent progresses in the turbulence flow modeling in porous media, which can be considered in the development of a better turbulence model for CFD simulations in condensers. The base of these turbulence

models is to volume-average and time-average the equations, in different orders, to reach macroscopic equation which can be used for engineering applications. These macroscopic equations include additional source terms that account for extra turbulence production and dissipation rate due to the presence of porous medium [28-31].

In addition to the extra source terms that take the effect of tube bundles into consideration, the influence of the dispersed phase (condensate droplets) on the two-phase turbulence equations is also important and needs to be studied. Two different approaches were usually used based on the literature to account for the turbulence induced by the dispersed phase in the Eulerian framework. In the first approach, the contribution of bubbles or droplets to the turbulence is simply added to the effective viscosity formulation and the turbulence equations remain unchanged [32]. In the second approach, the effect of dispersed phase is added as a source term to the primary phase turbulence equations. In this study, the latter approach is employed as it is more accurate and includes more details for the CFD analysis [33]. Various models proposed by different researchers [34-36] are studied and compared in the current work.

This chapter is organized as follows: Section 2.2 is devoted to introduce the theory of heat and mass transfer process in a shell and tube condenser, and the turbulence models are introduced in Section 2.3. Next, the computational set up is introduced in Section 2.4. The geometry and operating parameters, mesh generation, boundary conditions and problem description are all discussed in this section. In Section 2.5, the results are presented and discussed, and finally, conclusion and future work are given in Section 2.6.

2.2 Theory

Due to large number of tubes in a condenser, the porous media concept is used for the simulation of condensers in this study. The tube bundle region is modeled as a porous media with distributed resistance for both gas-phase and liquid-phase flows. The porosity, α, is defined as ratio of the volume occupied by the fluid to the total volume and its formula is given as follows for a tube bundle with a staggered arrangement:

$$
\begin{cases}
\alpha = 1 & \text{For non-tube bundle region} \\
\alpha = 1 - \dfrac{\pi}{2\sqrt{3}}\left(\dfrac{D_{od}}{P_t}\right)^2 & \text{For tube bundle region}
\end{cases}
\tag{2.1}
$$

where D_{od} and P_t are the tube outer diameter and pitch, respectively.

2.2.1 Governing equations

The mass condensation rate $\dot{m}$ is added as the sink and source terms to the gas-phase and liquid-phase continuity equations, respectively.

$$
\begin{aligned}
&\frac{\partial}{\partial t}\left(\beta_g \rho_g\right) + \nabla \cdot \left(\beta_g \rho_g \vec{V}_g\right) = -S_{mass} \\
&\frac{\partial}{\partial t}\left(\beta_l \rho_l\right) + \nabla \cdot \left(\beta_l \rho_l \vec{V}_l\right) = S_{mass} \\
&S_{mass} = \dot{m} \\
&\beta_g + \beta_l = \alpha
\end{aligned}
\tag{2.2}
$$

where β_l and β_g are the liquid and gas volume fractions and they represent the volume of the fluid occupied by liquid and gas, respectively.

Momentum source and sink terms to account for the effects of condensation, resistance force due to the presence of the tube bundle and interphase drag are added as source terms to the momentum equations for both gas and liquid phases. Gravity force is only considered for the liquid phase as its effect is almost negligible for the gas phase.

$$
\begin{aligned}
&\frac{\partial}{\partial t}\left(\beta_g \rho_g \vec{V}_g\right) + \nabla \cdot \left(\beta_g \rho_g \vec{V}_g \vec{V}_g\right) = -\beta_g \nabla p + \nabla \cdot \overline{\overline{\tau}}_g + S_{mom-g} \\
&\frac{\partial}{\partial t}\left(\beta_l \rho_l \vec{V}_l\right) + \nabla \cdot \left(\beta_l \rho_l \vec{V}_l \vec{V}_l\right) = -\beta_l \nabla p + \nabla \cdot \overline{\overline{\tau}}_l + S_{mom-l} \\
&S_{mom-g} = -\dot{m}\vec{V}_g + Rb_g + Wb_g \\
&S_{mom-l} = \dot{m}\vec{V}_l + \beta_l \rho_l \vec{g} + Rb_l + Wb_l
\end{aligned}
\tag{2.3}
$$

where Rb_g and Rb_l are the tube bundle resistance force for the gas and liquid phases, respectively, and are given in Eq. (2.4) as follows according to [37]. Pressure is assumed

common to both phases, and the mixture of vapor and air (non-condensable gases) is considered to be an ideal gas to define the properties for the gas mixture.

$$Rb_{xm} = \left(\beta \xi \rho u U\right)_m$$
$$Rb_{ym} = \left(\beta \xi \rho v U\right)_m$$
$$\xi = 2\left(\frac{f}{P_t}\right)\left(\frac{P_t \beta}{P_t - D_{od}}\right)^2 \left(\frac{1-\beta}{1-\beta_t}\right) \tag{2.4}$$
$$f = \begin{cases} 0.619\,\text{Re}_m^{-0.198} & \text{Re}_m < 8000 \\ 1.156\,\text{Re}_m^{-0.2647} & 8000 < \text{Re}_m < 2\times 10^5 \end{cases}$$
$$\text{Re}_m = \frac{\rho_m U_m D_{od}}{\mu_m}$$

where the subscript m is the phase indicator and refers to either liquid or gas phase, ξ is the pressure loss coefficient and f is the friction factor.

The terms Wb_g and Wb_l in Eq. (2.3) represent the interphase friction between the gas and liquid phases and are defined as follows as given in [6]:

$$Wb_{xg} = -Wb_{xl} = C_{fx}\left(u_l - u_g\right)$$
$$Wb_{yg} = -Wb_{yl} = C_{fy}\left(v_l - v_g\right)$$
$$C_{fx} = \frac{1}{2}\rho_g f_d A_d \left|u_l - u_g\right| \tag{2.5}$$
$$C_{fy} = \frac{1}{2}\rho_g f_d A_d \left|v_l - v_g\right|$$
$$A_d = \frac{1.5\beta_l}{D_d}$$

In which A_d is the total interphase area of droplets in the control volume, D_d is the droplet diameter that is taken to be 0.001 and f_d is the fiction factor, defined as follows as suggested by Clift et al. [38]:

$$f_d = \frac{24}{\text{Re}_p}\left(1+0.15\,\text{Re}_p^{0.687}\right) + \frac{0.42}{1+4.25\times10^4\,\text{Re}_p^{-1.16}} \qquad \text{Re}_p < 3\times10^5$$

$$\text{Re}_p = \frac{\rho_g D_d U_{rel}}{\mu_g} \tag{2.6}$$

$$U_{rel} = \sqrt{\left(u_g - u_l\right)^2 + \left(v_g - v_l\right)^2}$$

where Re_p is the Reynolds number based on the diameter of the droplets and relative velocity U_{rel}.

Finally, the local mass-fraction of the non-condensable gas (air) is predicted by solving the convection-diffusion equation for the air:

$$\frac{\partial}{\partial t}\left(\beta_g \rho_g \theta\right) + \nabla\cdot\left(\beta_g \rho_g \vec{V}_g \theta\right) = -\nabla\cdot\left(\beta_g \vec{J}\right) + \beta_g S_{diff} \tag{2.7}$$

The term θ is the air mass fraction in the above equation, J is the diffusion flux of the air in the vapor and S_{diff} is the source term.

2.2.2   Mass transfer modeling

The condensation rate is obtained by an overall energy balance between the shell side vapor-air mixture and the tube side cooling water.

$$\dot{m}LV_L = \frac{T - T_{cw}}{R_{total}} A \tag{2.8}$$

where L is the latent heat of condensation, A is the heat transfer area of the tubes located in each computational cell with volume V_L, and R_{total} is the total thermal resistance between the vapor and cooling water. There are several thermal resistances between the cooling water in the tube side and the vapor in the shell side. The total thermal resistance consists of the thermal resistance on the cooling water side (R_{cw}), tube wall resistance (R_{tw}), condensate film resistance (R_c) and thermal resistance due to the non-condensable gas layer (R_a). Both vapour and liquid condensate phases are assumed to be in the saturated state, and the vapor-air mixture temperature, T, is obtained according to the partial pressure of steam in the gas mixture.

$$R_{total} = R_{cw} + R_{tw} + R_c + R_a \tag{2.9}$$

The thermal resistance for the tube wall is obtained from the relation developed for cylindrical shell [39]:

$$R_{tw} = \frac{D_{od} \ln(D_{od}/D_{id})}{2\lambda_{tw}} \tag{2.10}$$

where D_{od} and D_{id} are the tube outer and inner diameters, respectively, and λ_{tw} is the thermal conductivity of the tube wall. To determine the thermal resistance on the cooling water side, Gnielinski correlation [40] is used:

$$R_{cw} = \frac{D_{od}}{D_{id}} \left(\frac{\lambda_{cw}}{D_{id}} \frac{\frac{f_R}{8} \left(\mathrm{Re}_{cw} - 1000 \right) \mathrm{Pr}_{cw}}{1 + 12.7 \left(\frac{f_R}{8} \right)^{0.5} \left(\mathrm{Pr}_{cw}^{2/3} - 1 \right)} \right)^{-1}$$

$$f_R = \left(0.79 \ln \left(\mathrm{Re}_{cw} \right) - 1.64 \right)^{-2} \tag{2.11}$$

$$\mathrm{Re}_{cw} = \frac{\rho_{cw} U_{cw} D_{id}}{\mu_{cw}}$$

$$\mathrm{Pr}_{cw} = \frac{\mu_{cw} C p_{cw}}{\lambda_{cw}}$$

where f_R is the Darcy friction factor, Re_{cw} and Pr_{cw} are the Reynolds and Prandtl numbers based on the cooling water flow properties. λ_{cw}, ρ_{cw}, μ_{cw}, Cp_{cw} and U_{cw} are the thermal conductivity, density, molecular viscosity, specific heat and velocity of the cooling water, respectively.

The thermal resistance due to the condensate film formed around the tube needs to be considered. The correlation used in this study is based on that given by Nusselt [41]:

$$Nu = \frac{hD_{od}}{\lambda_c} = 0.728 \left[\frac{gL\rho_c \left(\rho_c - \rho_g \right) D_{od}^{3}}{\mu_c \lambda_c \left(T_{ci} - T_{ow} \right)} \right]^{1/4} \tag{2.12}$$

λ_c, ρ_c and μ_c in Eq. (2.12) represent the condensate thermal conductivity, density and molecular viscosity, respectively, and T_{ci} and T_{ow} are temperatures at the condensate-vapor interface and tube outside wall. The Nusselt correlation given in Eq. (2.12) does not consider the vapor shear and inundation effects. In order to increase the accuracy of the correlation for the film condensation, the effects of the vapor shear and inundation have to be included in the analysis. In this study, the relation obtained by Berman and Tumanov [42] is used to model the effect of the vapor shear:

$$R_c' = \left(\frac{\lambda_c}{D_{od}} Nu \left(1 + 0.0095 \, \mathrm{Re}_g^{11.8/\sqrt{Nu}} \right) \right)^{-1}$$

$$\mathrm{Re}_g = \frac{\rho_g U_g D_{od}}{\mu_g}$$

(2.13)

In the above equation, Nu is obtained from Eq. (2.12). Nonetheless, it is rarely to see a single tube condenser used in industrial applications. Industrial condensers usually contain a large number of tubes. Therefore, the condensate formed on the top tubes will fall onto the lower tubes due to gravity and in turn influences heat transfer characteristics of the lower tubes. The relation suggested by Fuks [43] is chosen to account for the inundation effect on forced convection heat transfer:

$$\frac{R_c}{R_c'} = \left(\frac{\gamma_{tot}}{\gamma_c} \right)^n$$

(2.14)

where γ_{tot} is the condensate leaving the control volume, and γ_c is condensation rate in the control volume. Different values were suggested for n in the literature. Fuks [43] take the value to be 0.07, while Grant [44] claimed that 0.223 fits the experimental data better. In this study, the correlation proposed by Hu and Zhang [45] is considered. They suggested a linear relation for $n = YB$. In which, Y is equal to 0 at top of tube bundle and it increases to one at the bottom, and B is a constant taken to be equal to 0.37.

Finally, another important factor that significantly deteriorates the heat transfer is the presence of non-condensable gases such as air. Although the condenser designs aim to minimize the amount of non-condensable gases leaking into the domain, unfortunately

this amount cannot be reduced to zero. Therefore, it is important to consider the thermal resistance due to the accumulation of non-condensable gases at the gas-liquid interface. Berman and Fuks [46] obtained an empirical relation for the heat transfer characteristics of steam-air mixture flowing in downward direction through tube bundles according to the following equation:

$$R_a = \left[\frac{aD}{D_{od}} \mathrm{Re}_g^{1/2} \left(\frac{p}{p - p_s} \right)^b p^{1/3} \left(\frac{\rho_s L}{T} \right)^{2/3} \frac{1}{(T - T_{ci})^{1/3}} \right]^{-1}$$

(2.15)

for $\mathrm{Re}_g > 350,$ $b = 0.6$ $\alpha = 0.52$ First Tube row

                                       $\alpha = 0.67$ Second Tube row

                                       $\alpha = 0.52$ Third and later Tube row

for $\mathrm{Re}_g < 350,$ $b = 0.7$ $\alpha = 0.52$

P_s and ρ_s in Eq. (2.15) are the vapor partial pressure in the gas mixture and density, respectively. Also, the gas-mixture free stream and interface temperatures are represented by T and T_{ci}, and the diffusivity of the air in the vapor is represented by D.

2.3   Turbulence Modeling

The first turbulence model that is selected in this study is the modified standard k-ε turbulence model [21], in which the effects of the tube bundles and dispersed phase on the primary phase turbulence are taken into consideration. The turbulence kinetic energy (k) and dissipation rate (ε) equations are given as follows:

$$\frac{\partial}{\partial t}\left(\beta_g \rho_g k\right) + \nabla \cdot \left(\beta_g \rho_g k \vec{V}_g\right) = \frac{\partial}{\partial x_j}\left[\beta_g \left(\mu + \frac{\mu_t}{\sigma_\varepsilon}\right)\frac{\partial k}{\partial x_j}\right] - \beta_g \rho_g \varepsilon + \beta_g G_k + S_k$$

$$\frac{\partial}{\partial t}\left(\beta_g \rho_g \varepsilon\right) + \nabla \cdot \left(\beta_g \rho_g \varepsilon \vec{V}_g\right) = \frac{\partial}{\partial x_j}\left[\beta_g \left(\mu + \frac{\mu_t}{\sigma_k}\right)\frac{\partial \varepsilon}{\partial x_j}\right] + \beta_g C_{1\varepsilon}\frac{\varepsilon}{k}G_k - \beta_g C_{2\varepsilon}\rho\frac{\varepsilon^2}{k}G_k + S_\varepsilon$$

(2.16)

where G_k is the turbulence kinetic energy generation, σ_k and σ_ε are the turbulent Prandtl number for k and ε, and $C_{1\varepsilon}$ and $C_{2\varepsilon}$ are constants. The extra source terms in the k and ε

equations, S_k and S_ε, are used to account for the effects of the tube bundles and dispersed phase on the primary phase turbulence and they are represented as follows:

$$S_k = Rb_k + Wb_k$$
$$S_\varepsilon = Rb_\varepsilon + Wb_\varepsilon$$

(2.17)

Rb_k and Rb_ε are the terms that account for the effect of tube bundle in k and ε of the primary vapor-gas mixture phase, respectively. Similarly, Wb_k and Wb_ε are the terms that account for the effect of condensate droplets on k and ε, respectively. Different approaches have been proposed in the literature to model these extra terms.

One approach to model the increase of the turbulent kinetic energy due to tube bundle uses the assumption that the rate at which the work is being done on the fluid by the tubes is equal to the extra turbulent kinetic energy production; similar to the way turbulent kinetic energy is generated at the walls [3, 21]. Therefore the source term for k and ε equation is given as follows:

$$Rb_k = Rb_{xg}|u| + Rb_{yg}|v|$$
$$Rb_\varepsilon = \frac{1.92\varepsilon Rb_k}{k}$$

(2.18)

Another approach available in the literature which is completely different from the one described above is to develop the time-volume averaged turbulence equation in porous media and consider the extra source terms that appear in the equation. The method has been developed by several researchers for general porous media [28, 30, 31], and it is being applied to condenser analysis for the first time in this study. Nakayama et al. [28] developed a two equation k-ε model to solve the transport equations for turbulent kinetic energy and dissipation rate based on the volume averaging method in the porous media, and quantified the extra production terms as:

$$Rb_k = 39\alpha^2(1-\alpha)^{5/2}\frac{U_g^3}{D_{od}}$$
$$Rb_\varepsilon = 411C_{2\varepsilon}\alpha^{5/2}(1-\alpha)^4\frac{U_g^4}{D_{od}^2}$$

(2.19)

Later, Nakayama and Kuwahara [30] proposed a new generalized two equation k-ε model which can be used for any homogeneous porous media without any prior knowledge, and they demonstrated that it can be applied to any complex system that involves cross flows in banks of cylinders, packed beds and rod bundles. The extra source terms in the turbulence equations are given here for this model:

$$
Rb_k = 1.75 \frac{(1-\alpha)}{\alpha} \frac{U_g^{\,3}}{D_{od}}
$$
$$
Rb_\varepsilon = 4.55 C_{2\varepsilon} \left(\frac{1-\alpha}{\alpha} \right)^2 \frac{U_g^{\,4}}{D_{od}^{\,2}}
$$

(2.20)

In Eqs. (2.19) and (2.20), α is the porosity of the tubular region, $C_{2\varepsilon}$ is a constant equal to 1.92 and D_{od} is the tube outer diameter.

Another factor that needs to be considered is the effect of the dispersed phase on the primary phase turbulence. The approach that is widely used by many researchers [21, 33-36] is based on the premise that the energy lost by the droplet due to the drag is converted to the turbulent kinetic energy, therefore, the source term is expressed by the production of the drag force and relative velocity of the droplet:

$$
Wb_k = \beta_g C_{phase} \left[Wb_{xg} \left(u_l - u_g \right) + Wb_{yg} \left(v_l - v_g \right) \right]
$$
$$
Wb_\varepsilon = C_{\varepsilon_B} \frac{Wb_k}{\tau}
$$

(2.21)

where C_{phase} is the interphase exchange coefficient and taken to be 0.7 according to [21], Wb_{xg} and Wb_{yg} are the interphase drag forces given by Eq. (2.5). The turbulence dissipation source term, Wb_ε, depends on the time-scale τ and a coefficient $C_{\varepsilon b}$ which are different for different models. The choices of time scales and coefficients in different models are summarized in Table 2-1 as reported in [33].

There are many modifications proposed for the standard k-ε model. Two of the most popular ones are Realizable k-ε [24] and RNG k-ε [25] and they are considered in this study. The transport equations for the Realizable k-ε model and RNG k-ε model can be found in [47].

Table 2-1: Time scales and coefficients for different models

	Hu and Zhang [21]	Morel [34]	Troshko and Hassan [35]	Rzehak [33]
τ	k/ε	D_d/U_{rel}	$D_d/\sqrt{k}$	$\left(D_d^{\,2}/\varepsilon\right)^{1/3}$
C_{ε_B}	1.44	0.45	2.0	2.0

In addition to different k-ε models, the k-ω [26] and k-ω shear-stress transport (SST) [27] turbulence models are also tested in this study. The k-ω model is an empirical model based on the model transport equations for the turbulence kinetic energy and specific dissipation rate (ω). The equations for the k-ω model are given as:

$$\frac{\partial}{\partial t}\left(\beta_g \rho_g k\right) + \nabla \cdot \left(\beta_g \rho_g k \vec{V}_g\right) = \frac{\partial}{\partial x_j}\left[\beta_g \Gamma_k \frac{\partial k}{\partial x_j}\right] - \beta_g Y_k + \beta_g G_k$$

$$\frac{\partial}{\partial t}\left(\beta_g \rho_g \omega\right) + \nabla \cdot \left(\beta_g \rho_g \omega \vec{V}_g\right) = \frac{\partial}{\partial x_j}\left[\beta_g \Gamma_\omega \frac{\partial \omega}{\partial x_j}\right] + \beta_g G_\omega - \beta_g Y_\omega$$

(2.22)

where Γ_k and Γ_ε represent effective diffusivity of k and ε, and the terms Y_k and Y_ε represent dissipation of k and ω due to turbulence. The k-ω SST model [27] combines the strength of the k-ε model in the free stream region and the strength of the k-ω model in recirculating regions.

It is important to take note that the models mentioned above do not solve for detailed turbulence kinetic energy generated in the boundary layer around each tube and their accuracy is limited to the approximations imbedded in the porous medium and distributed flow resistance models.

2.4 Computational Method

The quasi-three-dimensional CFD simulations are performed using ANSYS FLUENT version 14.5 [47]. The test case used to evaluate the performance of the CFD models is an experimental shell and tube condenser [48], as shown in Figure 2-1. The geometric and operating parameters of this condenser are given in Table 2-2.

In the quasi-three-dimensional approach, the condenser is divided into several sectors along the cooling water flow direction, as shown in Figure 2-1, and the three-dimensionality effects are only considered due to the change of the cooling water temperature from one sector to next. That is, the inlet temperature of cooling water in each sector is set to be equal to the outlet cooling temperature of the previous sector. Therefore, a two-dimensional simulation is performed in each sector and the cooling water temperature is updated from one sector to next.

The rectangular tube bank is composed of 20 by 20 tubes of staggered arrangement as shown in Figure 2-1. The non-condensable gases and the remaining vapor leave the domain through a vent located on the centerline approximately two-third of the way into the tube bundle. In the venting area three tubes are removed and two sparge tubes are used to remove the non-condensed steam and air by suction.
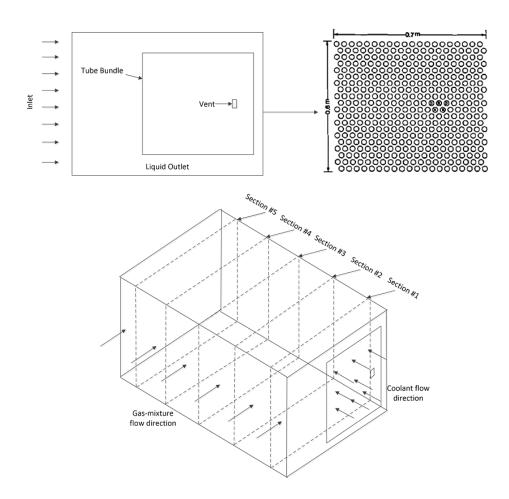
Figure 2-1: Configuration of the experimental condenser

Table 2-2: Geometric and operating parameters of the experimental condenser

Geometric parameters	
Number of tubes	400
Condenser length (m)	1.219
Condenser depth (m)	1.02
Condenser height (m)	0.78
Tube outer diameter (mm)	25.4
Tube wall thickness (mm)	1.25
Tube pitch (mm)	34.9
Operating parameters	
Inlet cooling water temperature (C)	17.8
Inlet cooling water velocity (m/s)	1.19
Inlet steam pressure (Pa)	27670
Inlet steam flow rate (kg/s)	2.032
Inlet air flow rate (Kg/s)	2.48e-04

2.4.1   Mesh

The ICEMCFD software is used to create the structured, two-dimensional mesh for the simulation. There are three separate zones in the computational domain, the tube region, vent and none-tube region, as shown in Figure 2-2. In the tubular region, all the tubes are uniformly distributed. Condensation only takes place in the tubular region that is a reasonable assumption knowing film condensation is the dominant mode of condensation in this condenser. All remaining vapor alongside non-condensable gases are being extracted from the domain at the vent. No condensation occurs in the none-tube region.
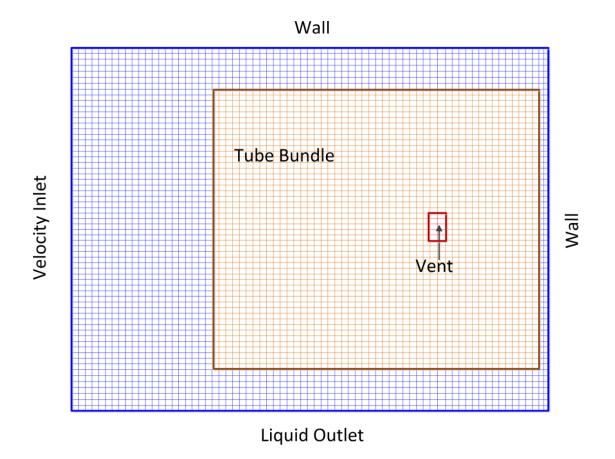
Figure 2-2: Two-dimensional mesh generated for condenser simulations

2.4.2   Boundary conditions

The boundary conditions for walls, outlet, inlet and vent are specified as follows:

Inlet: Uniform velocity with specified air mass fraction is used.

Outlet: Outlet condition for the liquid phase and a free-slip wall for the gas-phase are used. This condition is necessary in order to make sure liquid is the only phase leaving the domain due to gravity. It is required to use the user defined functions (UDFs) for this purpose as it is not a built-in boundary condition in FLUENT.

Wall: The top and right boundaries of the domain are treated as wall with no-slip condition.

Vent: Vent extracts the remaining vapor and all the non-condensable gases that entered the domain. It is modeled as a mass sink. The air mass fraction at the vent is obtained accordingly.

2.4.3   Solution Procedure

Eulerian-Eulerian multiphase model (two-fluid model) is used in this study to solve the two phase flow and heat transfer. That is, both liquid and gas phases are considered as the continuous media, therefore, separate conservation equations are solved for each phase. The effect of the secondary phase (liquid) on the primary phase (vapour-air mixture) is accounted for by adding source terms to the momentum and turbulence transport equations using UDFs. The effect of the tube bundle is considered by the porous media approach and the distributed flow resistance is added to the momentum equations using UDFs. The extra source terms to account for the effects the tube bundle and dispersed phase on the primary phase turbulence are added to the standard turbulence transport equations in ANSYS FLUENT by UDFs.

The simulations are performed using coupled solver for pressure–velocity coupling with very low Courant number (0.1). First order upwind calculation scheme is chosen for the discretization of momentum, energy, volume fraction, turbulent kinetic energy and dissipation rate equations.

2.5   Results and Discussion

The First, the performance of the numerical models is assessed using the original form of different turbulence models, i.e. without the extra source terms, the standard k-ε, RNG k-ε, Realizable k-ε, standard k-ω and k-ω SST models. In order to make this comparison, the experimental data from [48] is used. The average heat fluxes on the tubes are computed and compared with the experiments to determine which turbulence model has the best performance. These average fluxes are taken at four different locations on the tube bundle, the 3rd, 8th, 13th and 18th rows from the bottom of the tube bundle, to ensure all the features of the condenser at top, bottom and the middle of the tubular region are accounted for. As it can be seen from Figure 2-3, the k-ω SST method provides the best result among all the turbulence models considered, and RNG k-ε model is the best among all the k-ε models. The overall errors of the models in comparison with the experimental data are given in Table 2-3.
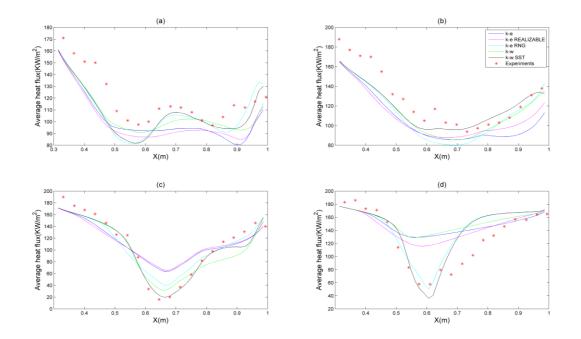
Figure 2-3: Performance evaluation of the standard turbulence models without extra source terms, (a) 3rd row tubes, (b) 8th row tubes, (c) 13th row tubes, and (d) 18th row tubes from the bottom of the tube bundle.

Table 2-3: Comparison of overall errors for the standard turbulence models

	k-ε	RNG k-ε	Realizable k-ε	k-ω	k-ω SST
% error	27.81%	17.36%	27.04%	19.54%	12.17%

Different approaches to model the effect of the porous region (the tube region) and liquid droplets on the gas phase turbulence are assessed. First, only the source terms accounting for the porous region effect on the turbulence kinetic energy and dissipation rate (Rb_k and Rb_ε) are added to the standard k-ε model and the three difference approaches to calculate Rb_k and Rb_ε given in Eqs. (2.18) to (2.20) are used. The results are presented in Figure 2-4 and Table 2-4. As it can be seen, the difference between the results from the three models is less than 1%. The model proposed by Hu and Zhang [21] provides the least average error. However, the Nakayama and Kuwahara model [30] predicts the trends really well compared with the experimental data and is the most stable solution with respect to others which can be a significant factor in simulating more complex condenser configurations, therefore, is selected as the most effective model.
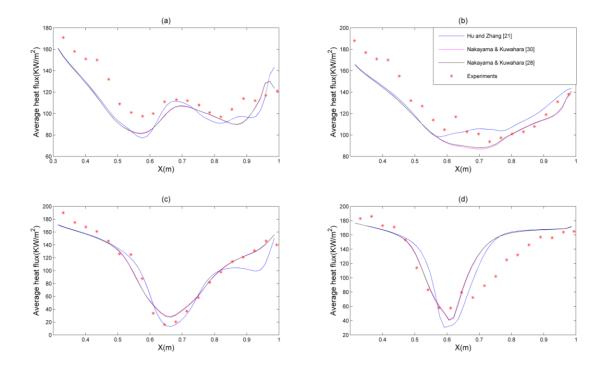
Figure 2-4: Performance evaluation of *k-ε* turbulence models considering the effect of tube bundle on the turbulence, (a) 3rd row tubes, (b) 8th row tubes, (c) 13th row tubes, and (d) 18th row tubes from the bottom of the tube bundle.

Table 2-4: Comparison of overall errors for the turbulence models accounting for the effect of the tube bundle on the turbulence

	Hu and Zhang [21]	Nakayama and Kuwahara [28]	Nakayama and Kuwahara [30]
% error	12.87%	13.61%	13.25%

After choosing the most effective turbulence model to account for the presence of tube bundles, it is also important to quantify the turbulence augmentation due to the presence of the dispersed liquid phase. The four different models listed in Table 2-1 to calculate Wb_k and Wb_ε are used. These four models are compared with respect to the experiments and the results are given in Figure 2-5 and Table 2-5.
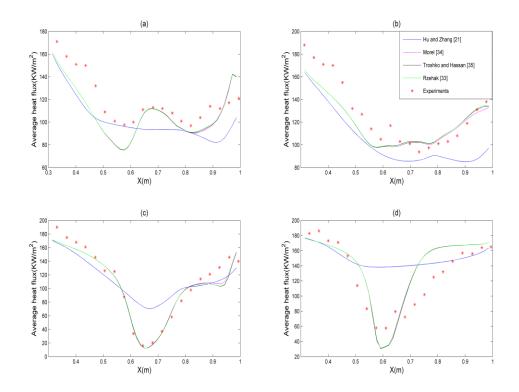
Figure 2-5: Performance evaluation of *k-ε* turbulence models considering the effect of the dispersed phase on turbulence, (a) 3rd row tubes, (b) 8th row tubes, (c) 13th row tubes, and (d), 18th row tubes from the bottom of the tube bundle.

Table 2-5: Comparison of overall errors for the turbulence models accounting for the effect of the dispersed phase on turbulence

	Hu and Zhang [21]	Morel [34]	Troshko and Hassan [35]	Rzehak [33]
% error	30.32%	12.42%	12.58%	12.53%

By looking at the results reported in the Figure 2-5 and Table 2-5, it can be concluded that although the errors are quite similar between the models by Morel [34], Troshko and Hassan [35], and Rzehak [33], the model proposed by Morel [34] gives the most accurate result.

It is important to consider the effects of both the tube bundle and liquid droplets on the gas phase turbulence simultaneously to capture the physics of the phenomena. Therefore, source terms representing both effects are added to turbulence transport equations, and the model by Nakayama and Kuwahara [30] for the tube bundle effect and the model by Morel [34] for the liquid droplets effect are selected. Therefore, the modified standard k-ε and RNG k-ε models are proposed in this study by adding the additional source terms into those models for the simulation the two-phase flows in condensers. The results from the modified standard k-ε and RNG k-ε models are also compared with the k-ω SST as well as the previous work done by Hu and Zhang [45] as shown in Table 2-6 and Figure 2-6.
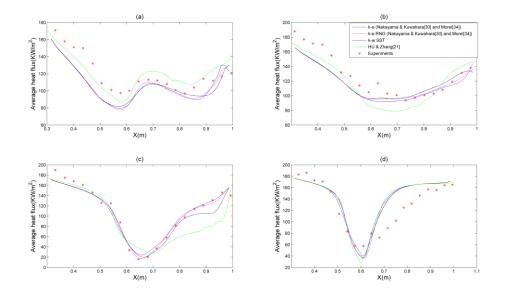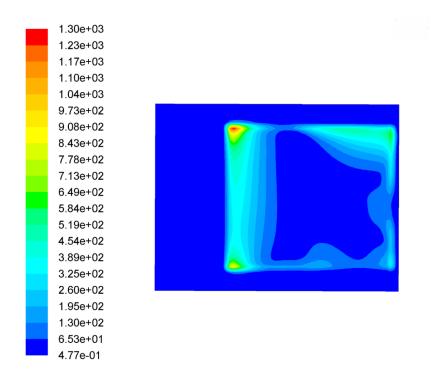
Figure 2-6: Performance evaluation of the turbulence models in comparison with the previous work [45], (a) 3rd row tubes, (b) 8th row tubes, (c) 13th row tubes, and (d), 18th row tubes from the bottom of the tube bundle.

Table 2-6: Comparison of overall errors for the modified turbulence models and the previous work [45].

	Hu and Zhang [45]	k-ε (With source terms)	RNG k-ε (With source terms)	k-ω SST
% error	17.01%	12.42%	11.35%	12.17%

The results demonstrate that the modified RNG k-ε model reduces the error from 17.36% by the original RNG k-ε model to 11.35% and the modified standard k-ε model reduces the error from 27.81% by the original model to 12.42%. The modified RNG k-ε model gives the best result. On the other hand, the error by the k-ω SST model is similar to those from the modified standard k-ε and modified RNG k-ε models although it is a little bit higher than that from the modified RNG k-ε model, and it is the best model among the standard models without the extra source terms. In addition, the comparison with the results from the previous work by Hu and Zhang [45], where a different modified k-ε model was used, demonstrates the error from the current modified k-ε model is 27% lower than the model from [45] and the error from the current modified RNG k-ε model is 33% lower than the model from [45]. Moreover, the models proposed in this study are computationally more stable than the previous one from [21].

The rest of the section is devoted to analyze the results obtained from the best model, the modified RNG k-ε model. First, the contours of turbulent kinetic energy and dissipation rate are shown in Figure 2-7 and Figure 2-8, respectively. It is clear from the figures that both the turbulent kinetic energy and dissipation rate are increased where the vapor-gas mixture enters the tubular region. The reason for this is that the velocity of the mixture is at its maximum in the entrance of the tubular region since the flow area is reduced due to the presence of the tubes. Then, the gas phase velocity decreases due to the condensation in the tube bundle region. However, this is an approximation that is limited by the errors introduced by modeling the tube bundle region using porous media and should be treated with cautious.

Figure 2-7: Turbulent kinetic energy contour in Section #1 using the modified RNG k-ε model
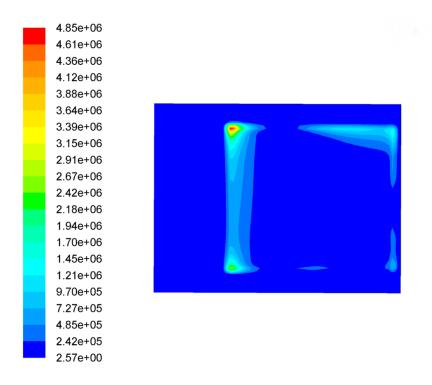
Figure 2-8: Turbulent dissipation rate contour in Section #1 using the modified RNG k-ε model

The heat transfer rate contour is provided in Figure 2-9. As it was expected, the heat transfer between the two shell size and tube side is maximum as the vapor-air mixture enters the tubular region. The reason for this increase is the higher vapor velocity, and as the vapor slows down deeper into the tube region due to condensation, heat and mass transfer will also decrease. Moreover, two regions in the tube bundle have relatively lower heat transfer rate. They are located near the vent and at the bottom of tubular region. The reason for the lower heat transfer near the vent is the accumulation of the non-condensable gases in that area, which will increase the thermal resistance resulting in a decrease in the heat transfer rate. The accumulation of non-condensable gases near the vent is shown in Figure 2-10. Also, the reason behind the reduction in heat transfer at the bottom of the tubular region is that the condensate formed around the tubes falls from the top due to gravity on the lower tubes and increases the thickness of the condensate film around them. This phenomenon called inundation increases the thermal resistance due to condensate film, and decreases the heat transfer. A closer look at the liquid volume fraction (Figure 2-11) shows that the regions with lower heat transfer rate at the bottom of the tubular region corresponds to the higher liquid volume fraction.
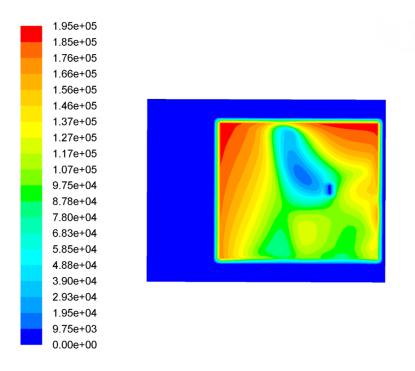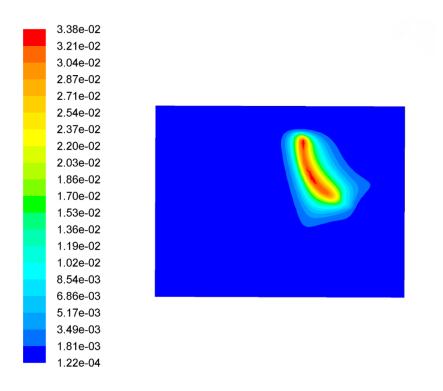
Figure 2-9: Heat transfer rate contour in Section #1 using the modified RNG k-ε model

Figure 2-10: Air mass-fraction contour in Section #1 using the modified RNG *k-ε* model
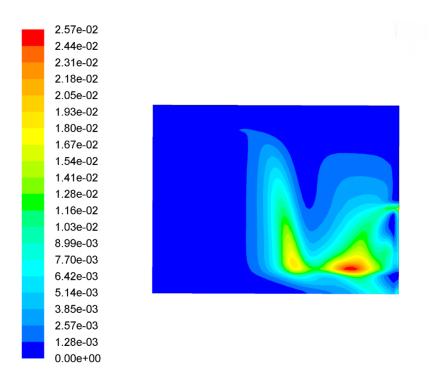
Figure 2-11: Volume fraction of liquid contour in Section #1 using the modified RNG *k-ε* model

2.6 Conclusion

The computational fluid dynamic analysis of the two-phase flow and heat transfer in a steam surface condenser has been carried out. Eulerian-Eulerian two-phase model was selected for the simulation, and the quasi-three-dimensional model was adopted to account for the temperature changes in the coolant flow. The porous media approach with the distributed resistance due to the presence of tubes in the condenser was used.

Several turbulence models from the k-ε and k-ω families were assessed to select the most effective model for the simulation of two-phase flow and heat transfer in tube and shell condensers. The k-ω SST had the best performance and the least error among different turbulence models without additional source terms accounting for the effects of tube bundles and two-phase interactions on the gas-phase turbulence.

However, it is vital to consider tube bundle and secondary phase (liquid droplets) effects, and single phase turbulence transport equations toned to be modified to capture the physics of the flow phenomenon in tube and shell condensers. Therefore, various models, which consider the turbulence augmentation due to tube bundle region and secondary phase, were tested to select the most effective models. Finally, the modified standard k-ε and RNG k-ε models are proposed that account for the turbulence augmentation around the tubes and liquid droplets. The proposed models were tested against the experimental data. Comparisons were also made with the previous work and other available models, which demonstrated significant improvement of the proposed models.

References

[1]   S. Kakac, H. Liu, and A. Pramuanjaroenkij, *Heat exchangers: selection, rating, and thermal design*: CRC press, 2012.

[2]   V. K. Patel and R. V. Rao, "Design optimization of shell-and-tube heat exchanger using particle swarm optimization technique," *Applied Thermal Engineering,* vol. 30, pp. 1417-1425, 2010.

[3]   M. Prithiviraj and M. J. Andrews, "Three dimensional numerical simulation of shell-and-tube heat exchangers. Part I: foundation and fluid mechanics," *Numerical Heat Transfer, Part A: Applications,* vol. 33, pp. 799-816, 1998.

[4]   S. Patankar and D. Spalding, "Heat exchanger design theory source book," *Scripta Book Co., Washington, DC,* pp. 155-176, 1974.

[5]   M. Prithiviraj and M. Andrews, "Three-dimensional numerical simulation of shell-and-tube heat exchangers. Part II: Heat transfer," *Numerical Heat Transfer, Part A Applications,* vol. 33, pp. 817-828, 1998.

[6]   H. G. Hu and C. Zhang, "Evaluations of closure correlations for the simulation of two-phase flows in condensers," *Heat Transfer Engineering,* vol. 30, pp. 437-451, 2009.

[7]   C. Zhang, "Numerical modeling using a quasi-three-dimensional procedure for large power plant condensers," *Journal of heat transfer,* vol. 116, pp. 180-188, 1994.

[8]   C. Zhang, A. Sousa, and J. Venart, "The numerical and experimental study of a power plant condenser," *Journal of heat transfer,* vol. 115, pp. 435-445, 1993.

[9]   B. Davidson and M. Rowe, "Simulation of power plant condenser performance by computational methods: an overview," *Power Condenser Heat Transfer Technology,* pp. 17-49, 1981.

[10]   C. Zhang and A. Bokil, "A quasi-three-dimensional approach to simulate the two-phase fluid flow and heat transfer in condensers," *International journal of heat and mass transfer,* vol. 40, pp. 3537-3546, 1997.

[11]   I. S. Ramón and M. P. González, "Numerical study of the performance of a church window tube bundle condenser," *International journal of thermal sciences,* vol. 40, pp. 195-204, 2001.

[12]   M. Prieto, I. Suarez, and E. Montanes, "Analysis of the thermal performance of a church window steam condenser for different operational conditions using three models," *Applied thermal engineering,* vol. 23, pp. 163-178, 2003.

[13]   R. Roy, V. Gokhale, and M. Ratisher, "A computational model of a power plant steam condenser," *Journal of energy resources technology,* vol. 123, pp. 81-91, 2001.

[14]   A. Rusowicz, "The numerical modeling and measurements for power plant condenser," 2009.

[15]   M. R. Malin, "Modelling flow in an experimental marine condenser," *International Communications in Heat and Mass Transfer,* vol. 24, pp. 597-608, 1997.

[16]   A. Bush, G. Marshall, and T. Wilkinson, "The prediction of steam condensation using a three component solution algorithm," in *Proceedings of the Second International Symposium on Condensers and Condensation, University of Bath, UK*, 1990, pp. 223-234.

[17]   S. B. Beale, "A Simple, Effective Viscosity Formulation for Turbulent Flow and Heat Transfer in Compact Heat Exchangers," *Heat Transfer Engineering,* vol. 33, pp. 4-11, 2012.

[18]   A. Gómez, N. Fueyo, and L. I. Díez, "Modelling and simulation of fluid flow and heat transfer in the convective zone of a power-generation boiler," *Applied Thermal Engineering,* vol. 28, pp. 532-546, 2008.

[19]   W. Sha, T. Kao, S. Cho, and C. Yang, "Multidimensional numerical modeling of heat exchangers," *Journal of Heat Transfer,* vol. 104, pp. 417-425, 1982.

[20]   Y. You, A. Fan, S. Huang, and W. Liu, "Numerical modeling and experimental validation of heat transfer and flow resistance on the shell side of a shell-and-tube heat exchanger with flower baffles," *International Journal of Heat and Mass Transfer,* vol. 55, pp. 7561-7569, 2012.

[21]   H. G. Hu and C. Zhang, "A modified k–ε turbulence model for the simulation of two-phase flow and heat transfer in condensers," *International Journal of Heat and Mass Transfer,* vol. 50, pp. 1641-1648, 2007.

[22]   Y. He, W. Tao, B. Deng, X. Li, and Y. Wu, "Numerical simulation and experimental study of flow and heat transfer characteristics of shell side fluid in shell-and-tube heat exchangers," in *Proceedings of Fifth International Conference on Enhanced, Compact and Ultra-Compact Heat Exchangers: Science, Engineering and Technology, Hoboken, NJ, USA*, 2005, pp. 29-42.

[23]   H. Zeng, J. a. Meng, and Z. Li, "Numerical study of a power plant condenser tube arrangement," *Applied Thermal Engineering,* vol. 40, pp. 294-303, 2012.

[24]   T.-H. Shih, W. Liou, A. Shabbir, Z. Yang, and J. Zhu, "A new k-epsilon eddy viscosity model for high Reynolds number turbulent flows: Model development and validation," *NASA STI/Recon Technical Report N,* vol. 95, p. 11442, 1994.

[25]   V. Yakhot and S. A. Orszag, "Renormalization-group analysis of turbulence," *Physical review letters,* vol. 57, p. 1722, 1986.

[26]   D. C. Wilcox, *Turbulence modeling for CFD* vol. 2: DCW industries La Canada, CA, 1998.

[27]   F. R. Menter, "Two-equation eddy-viscosity turbulence models for engineering applications," *AIAA journal,* vol. 32, pp. 1598-1605, 1994.

[28]   F. Kuwahara, Y. Kameyama, S. Yamashita, and A. Nakayama, "Numerical modeling of turbulent flow in porous media using a spatially periodic array," *Journal of Porous Media,* vol. 1, 1998.

[29]   M. H. Pedras and M. J. de Lemos, "Macroscopic turbulence modeling for incompressible flow through undeformable porous media," *International Journal of Heat and Mass Transfer,* vol. 44, pp. 1081-1093, 2001.

[30]   A. Nakayama and F. Kuwahara, "A general macroscopic turbulence model for flows in packed beds, channels, pipes, and rod bundles," *Journal of Fluids Engineering,* vol. 130, p. 101205, 2008.

[31]   F. E. Teruel, "Numerical computation of macroscopic turbulence quantities in representative elementary volumes of the porous medium," *International Journal of Heat and Mass Transfer,* vol. 53, pp. 5190-5198, 2010.

[32]   Y. Sato, M. Sadatomi, and K. Sekoguchi, "Momentum and heat transfer in two-phase bubble flow—I. Theory," *International Journal of Multiphase Flow,* vol. 7, pp. 167-177, 1981.

[33]   R. Rzehak and E. Krepper, "Bubble-induced turbulence: Comparison of CFD models," *Nuclear Engineering and Design,* vol. 258, pp. 57-65, 2013.

[34]   C. Morel, "Turbulence modeling and first numerical simulations in turbulent two-phase flows," in *Symposium on Turbulent Shear Flows, 11 th, Grenoble, France*, 1997.

[35]   A. Troshko and Y. Hassan, "A two-equation turbulence model of turbulent bubbly flows," *International Journal of Multiphase Flow,* vol. 27, pp. 1965-2000, 2001.

[36]   M. Politano, P. Carrica, and J. Converti, "A model for turbulent polydisperse two-phase flow in vertical channels," *International Journal of Multiphase Flow,* vol. 29, pp. 1153-1182, 2003.

[37]   D. Rhodes and L. Carlucci, *Predicted and measured velocity distributions in a model heat exchanger*: Chalk River Nuclear Laboratories, 1984.

[38]   R. Clift, J. R. Grace, and M. E. Weber, *Bubbles, drops, and particles*: Courier Dover Publications, 2005.

[39]   F. P. Incropera, A. S. Lavine, and D. P. DeWitt, *Fundamentals of heat and mass transfer*: John Wiley & Sons, 2011.

[40]   V. Gnielinski, "New equations for heat and mass transfer in the turbulent flow in pipes and channels," *NASA STI/Recon Technical Report A,* vol. 75, p. 22028, 1975.

[41]   W. Nusselt, "The condensation of steam on cooled surfaces," *Z. Ver. Dtsch. Ing,* vol. 60, pp. 541-546, 1916.

[42]   D. Chisholm, "Modern developments in marine condensers: Noncondensable gases: An overview," *Power Condenser Heat Transfer Technology,* pp. 95-142, 1981.

[43]   S. N. Fuks, "Heat transfer with condensation of steam flowing in a horizontal tube bundle," *Teploenergetika,* vol. 4, pp. 35-39, 1957.

[44]   I. D. R. Grant and B. D. J. Osment, *The Effect of Condensate Drainage on Condensor Performance*: National Engineering Laboratory, 1968.

[45]   H. G. Hu and C. Zhang, "A new inundation correlation for the prediction of heat transfer in steam condensers," *Numerical Heat Transfer, Part A: Applications,* vol. 54, pp. 34-46, 2008.

[46]   S. M. Ghiaasiaan, *Two-Phase Flow, Boiling, and Condensation: In Conventional and Miniature Systems*: Cambridge University Press, 2008.

[47]   "ANSYS FLUNET 14.5 Theory Guide," ANSYS Inc.

[48]   S. Al-Sanea, N. Rhodes, D. Tatchell, and T. Wilkinson, "A computer model for detailed calculation of the flow in power station condensers," in *Condensers: theory and practice. Symposium*, 1983, pp. 70-88.

Chapter 3

3 Three-Dimensional Numerical Model for the Two-Phase Flow and Heat Transfer in Condensers

3.1 Introduction

Condensers are commonly used in industrial applications. Most of them contain banks of thin-walled tubes and the steam condenses over or within these tubes through which the heat transfer occurs with the coolant. The condensate liquid formed during this process then falls under gravity into the condenser storage well [1].

In this study, the focus is on steam surface shell-and-tube condensers which are commonly used in power plant industry to condense the exhaust steam from the turbine to liquid water. The mixture of the steam and non-condensable gases (mainly air) flows in the shell-side and the condensation occurs outside of horizontal tubes through which the cooling water flows. There might be one or more partition plates used in the condenser to support the weight of the tube bank depending on the condenser and tubes design characteristics. These tube supports provide an air-tight fit, so that the shell-side fluid cannot pass through them.

The design of condensers has traditionally been conducted by experienced designers through trial and error approach based on previous designs, or tests [2-5]. However, a detailed knowledge of the flow field and heat transfer in condensers is required in order to design a reliable and efficient unit, and the traditional methods do not provide this level of details. One way to overcome this issue is to perform experimental tests; however, this type of experiments are usually expensive and time consuming [6]. Also detailed turbulence measurements and flow visualizations are difficult to perform if not impossible. Therefore, a reliable, robust numerical model can be a useful tool to provide further insight to the complex flow and heat transfer happening in an industrial condenser.

Several numerical models have been proposed to simulate flow and heat transfer in condensers. Patankar and Spalding [7] were pioneers in this field as they introduced the porous media concept to account for the drag force due to tube bundles, and consequently, the computational time can be significantly reduced as the numerical procedure does not require the detailed analysis of flow and temperature fields around each tube. Many numerical models have been developed based on the porous media concept with a reasonable accuracy [8-28]. These models can be classified into two main categories: single-phase and two-phase models.

In single-phase models, the effect of the second phase is neglected and it is assumed that the condensate disappears from the domain as it is formed. Davidson and Rowe [8] solved the single-phase equations and used Berman and Fuks correlation to account for the effect of non-condensable gases. Al-Sanea et al. [9], Malin [14], Roy et al. [15], Prieto et al. [16], Ormiston et al. [17, 18], and Zhang et al. [26] were among the first researchers who performed the simulations of condensers using single-phase models, in which the effects of the inundation and interphase interaction on the fluid flow were neglected. Zhang and Zhang [28] studied the sensitivity of the condensation heat transfer coefficient using a single-phase model. Zhang [16] studied the effects on the heat transfer rate due to the inundation, inlet air mass fractions, and cooling water flow rate using a single-phase model. He et al. [2] performed a three-dimensional single-phase analysis using a modified k-ε model for shell-and-tube heat exchangers. Nedelkovski et al. [29] developed a finite element method to solve three-dimensional single-phase equations for the condenser where the effect of non-condensable gases was considered. Later, Rusowicz [30] performed the simulation using a single-phase two-dimensional steady state model on a 50 MW plant condenser and reported satisfactory results. Zeng et al. [4] solved the single-phase mixture equation for the mixture of steam and non-condensable gases in addition to the RNG k-ε model to study the effect of different tube arrangements for a 300 MW power plant condenser.

Two-phase models regard both gas and liquid as continuous and interpenetrating fluids, and the interaction between the phases are modeled. The first model was developed by Al-Sanea et al. [10], in which they included the interphase effect in their two-phase

model. Rabas and Kassem [11] included the condensate inundation effect and neglected the vapor shear effect on the convective heat transfer in condensers. McNaught and Cotchin [12] implemented a new correlation to account for the effect of inundation. Bush et al. [13] predicted the flow and heat transfer in an experimental condenser using a two-phase model. Moreover, Zhang and Bokil [24] included the interphase effect and used a two-phase model to simulate a condenser. Hu and Zhang [19] developed a modified k-ε turbulence model for two-phase flows in condensers, and later assessed the effects of different closure correlation on the numerical simulations [20] and proposed a new correlation to account for the effect of the inundation on the convective heat transfer in condensers [21].

In this study, an Eulerian-Eulerian model for the two-phase flow and heat transfer in condensers will be developed alongside a robust turbulence model for the primary phase accounting for the extra turbulence kinetic energy generation and dissipation rate due to the presence of the tube bank and the condensate droplets. The mass and momentum conservation equations for both gas and liquid phases, and the species transport equation for the non-condensable gas are solved. The relevant correlations are selected based on previous studies to model the effect of the condensate inundation and non-condensable gases on the heat and mass transfer in condensers.

Moreover, the shell-side flow is three-dimensional due to the change in the cooling water temperature. On the other hand, the presence of the tube supports restricts the shell-side flow in the third direction. In the past, the majority of the researchers used two-dimensional or at most quasi-three-dimensional models for condenser simulations [19-21]. In this work, the three-dimensional multi-phase Eulerian-Eulerian model is adopted and the results are compared with the quasi-three-dimensional model to assess the effect of the three-dimensionality on the accuracy of the two-phase flow modeling in a condenser. Furthermore, the full three-dimensional two-phase CFD simulation is performed on a full-scale industrial condenser for the first time. The auxiliary relations and closure correlations are implemented in a commercial CFD code, ANSYS FLUENT, to model and analyze the complex flow and heat transfer in a condenser. The procedure to implement the closure correlations and auxiliary relationships necessary to model the

turbulent two phase flow in a condenser into a commercial CFD code is presented, which can be used to meet the numerical modeling and analysis needs of an industrial application.

This chapter is organized as follows: Section 3.2 is devoted to introduce the theory of the fluid flow, heat and mass transfer problem in a shell-and-tube condenser. The governing equations are presented in this section. Next, the numerical modeling procedure is introduced in Section 3.3. The geometry and operating parameters, mesh generation, boundary conditions and problem description are all discussed in this section. In Section 3.4, the results are presented and discussed. Two different approaches are taken to analyze the fluid flow and heat transfer in the condenser: (1) quasi-three-dimensional modelling and (2) three-dimensional modeling. The results from both approaches are provided in Section 3.5 and compared with the experimental data, and finally, conclusion and future work are given in Section 3.6.

3.2 Numerical Model

As it was stated before, the tube bank effect on the shell-side flow is modeled by the distributed flow resistance in the tubular region. The tubular region is represented as a porous medium. The porosity, α, is given as follows for the tube bundle with a staggered arrangement:

$$\begin{cases} \alpha = 1 & \text{For non-tube bundle region} \\ \alpha = 1 - \dfrac{\pi}{2\sqrt{3}}\left(\dfrac{D_{od}}{P_t}\right)^2 & \text{For tube bundle region} \end{cases} \tag{3.1}$$

where D_{od} and P_t are the tube outer diameter and pitch, respectively.

3.2.1   Governing equations

The Eulerian-Eulerian approach (two-fluid model) is used in this study. In this approach, the fluids of both phases are assumed to behave as continuous media and a set of conservation equations is solved for each phase.

The mass condensation rate $\dot{m}$ is added as the sink and source terms to the gas-phase and liquid-phase continuity equations, respectively.

$$\frac{\partial}{\partial t}\left(\beta_g \rho_g\right) + \nabla \cdot \left(\beta_g \rho_g \vec{V}_g\right) = -S_{mass}$$

$$\frac{\partial}{\partial t}\left(\beta_l \rho_l\right) + \nabla \cdot \left(\beta_l \rho_l \vec{V}_l\right) = S_{mass} \qquad (3.2)$$

$$S_{mass} = \dot{m}$$

$$\beta_g + \beta_l = \alpha$$

where β_g and β_l are the gas and liquid volume fractions, respectively, and their summation is equal to the porosity, which is defined as ratio of the volume occupied by the fluid to the total volume.

To account for the effects of the tube bundle resistance and interphase drag, source terms are added to the gas-phase and liquid-phase momentum equations. The source terms due to the mass transfer are also included in the momentum equations for both gas and liquid phases. The gravity force is only considered for the liquid phase as its effect is negligible for the gas phase:

$$\frac{\partial}{\partial t}\left(\beta_g \rho_g \vec{V}_g\right) + \nabla \cdot \left(\beta_g \rho_g \vec{V}_g \vec{V}_g\right) = -\beta_g \nabla p + \nabla \cdot \bar{\bar{\tau}}_g + S_{mom-g}$$

$$\frac{\partial}{\partial t}\left(\beta_l \rho_l \vec{V}_l\right) + \nabla \cdot \left(\beta_l \rho_l \vec{V}_l \vec{V}_l\right) = -\beta_l \nabla p + \nabla \cdot \bar{\bar{\tau}}_l + S_{mom-l} \qquad (3.3)$$

$$S_{mom-g} = -\dot{m}\vec{V}_g + Rb_g + Wb_g$$

$$S_{mom-l} = \dot{m}\vec{V}_l + \beta_l \rho_l \vec{g} + Rb_l + Wb_l$$

where Rb_g and Rb_l are the tube bundle resistance force for the gas and liquid phases, respectively, and are given as follows according to [31]:

$$Rb_{xm} = \left(\beta \xi \rho u U \right)_m$$

$$Rb_{ym} = \left(\beta \xi \rho v U \right)_m$$

$$Rb_{zm} = \left(\beta \xi \rho w U \right)_m$$

$$\xi = 2 \left(\frac{f}{P_t} \right) \left(\frac{P_t \beta}{P_t - D_o} \right)^2 \left(\frac{1 - \beta}{1 - \beta_t} \right)$$

$$f = \begin{cases} 0.619 \, \text{Re}_m^{-0.198} & \text{Re}_m < 8000 \\ 1.156 \, \text{Re}_m^{-0.2647} & 8000 < \text{Re}_m < 2 \times 10^5 \end{cases}$$

$$\text{Re}_m = \frac{\rho_m U_m D_d}{\mu_m}$$

(3.4)

where the subscript m is the phase indicator and refers to either liquid or gas, ξ is the pressure loss coefficient and f is friction factor.

The terms Wb_g and Wb_l in Eq. (3.3) represent the interphase friction between the gas and liquid phases and are defined as follows as given in [20]:

$$Wb_{xg} = -Wb_{xl} = C_{fx} \left(u_l - u_g \right)$$

$$Wb_{yg} = -Wb_{yl} = C_{fy} \left(v_l - v_g \right)$$

$$Wb_{zg} = -Wb_{zl} = C_{fz} \left(w_l - w_g \right)$$

$$C_{fx} = \frac{1}{2} \rho_g f_d A_d \left| u_l - u_g \right|$$

$$C_{fy} = \frac{1}{2} \rho_g f_d A_d \left| v_l - v_g \right|$$

$$C_{fz} = \frac{1}{2} \rho_g f_d A_d \left| w_l - w_g \right|$$

$$A_d = \frac{1.5 \beta_l}{D_d}$$

(3.5)

where A_d is the total interphase area of droplets in the control volume, D_d is the droplet diameter that is taken to be 0.001 and f_d is the fiction factor, defined as follows as suggested by Clift et al. [32]:

$$f_d = \frac{24}{\mathrm{Re}_p}\left(1+0.15\,\mathrm{Re}_p^{0.687}\right) + \frac{0.42}{1+4.25\times10^4\,\mathrm{Re}_p^{-1.16}} \qquad \mathrm{Re}_p < 3\times10^5$$

$$\mathrm{Re}_p = \frac{\rho_g D_d U_{rel}}{\mu_g} \tag{3.6}$$

$$U_{rel} = \sqrt{\left(u_g-u_l\right)^2 + \left(v_g-v_l\right)^2 + \left(w_g-w_l\right)^2}$$

where Re_p is the Reynolds number based on the diameter of the droplets and relative velocity U_{rel}.

Finally, the local mass-fraction of the non-condensable gases (air) is predicted in the condenser by solving the convection-diffusion equation for the air:

$$\frac{\partial}{\partial t}\left(\beta_g \rho_g \theta\right) + \nabla\cdot\left(\beta_g \rho_g \vec{V}_g \theta\right) = -\nabla\cdot\left(\beta_g \vec{J}\right) + \beta_g S_{diff} \tag{3.7}$$

where θ is the air mass fraction, J is the diffusion flux of the air in the vapor, and S_{diff} is the source term.

3.2.2   Condensation Modeling

The condensation rate is obtained by an overall energy balance between the shell-side vapor-air mixture and the tube-side cooling water.

$$\dot{m}LV_L = \frac{T-T_{cw}}{R_{total}} A \tag{3.8}$$

where L is the latent heat of condensation, A is the heat transfer area of the tubes located in each computational cell with volume V_L, and R_{total} is the total thermal resistance between the vapor and coolant. There are several thermal resistances between the cooling water in the tube side and the vapor in the shell side. The total thermal resistance consists of the thermal resistance on the cooling water side (R_{cw}), tube wall resistance (R_{tw}), condensate film resistance (R_c) and thermal resistance due to the non-condensable gas layer (R_a). Both vapour and liquid condensate phases are assumed to be in the saturated state, and the vapor-air mixture temperature, T, is obtained according to the partial pressure of steam in the gas mixture.

$$R_{total} = R_{cw} + R_{tw} + R_c + R_a \tag{3.9}$$

The thermal resistance for the tube wall is obtained from the relation developed for the cylindrical shell [33]:

$$R_{tw} = \frac{D_{od} \ln(D_{od}/D_{id})}{2\lambda_{tw}} \tag{3.10}$$

where D_{od} and D_{id} are the tube outer and inner diameters, respectively, and λ_{tw} is the thermal conductivity of the tube wall. To determine the thermal resistance on the cooling water side, Gnielinski correlation [34] is used:

$$R_{cw} = \frac{D_{od}}{D_{id}} \left(\frac{\lambda_{cw}}{D_{id}} \frac{\frac{f_R}{8}(\mathrm{Re}_{cw} - 1000)\mathrm{Pr}_{cw}}{1 + 12.7\left(\frac{f_R}{8}\right)^{0.5}\left(\mathrm{Pr}_{cw}^{2/3} - 1\right)} \right)^{-1}$$

$$f_R = \left(0.79\ln\left(\mathrm{Re}_{cw}\right) - 1.64\right)^{-2} \tag{3.11}$$

$$\mathrm{Re}_{cw} = \frac{\rho_{cw} U_{cw} D_{id}}{\mu_{cw}}$$

$$\mathrm{Pr}_{cw} = \frac{\mu_{cw} Cp_{cw}}{\lambda_{cw}}$$

where f_R is the Darcy friction factor, Re_{cw} and Pr_{cw} are the Reynolds and Prandtl numbers based on the cooling water flow properties. λ_{cw}, ρ_{cw}, μ_{cw}, Cp_{cw} and U_{cw} are the thermal conductivity, density, molecular viscosity, specific heat and velocity of the cooling water, respectively.

Unlike the thermal resistances for the tube wall and cooling water flow, finding the thermal resistance due to the condensate film formed around the tubes is not straightforward. The pioneering work on the film condensation field was done by Nusselt [35]. Although his analysis included several assumptions to simplify the governing equations and boundary conditions of the problem and the range in which its results are accurate is very limited, it laid the foundation for the theoretical analysis of condensing films and future improvements by other researchers. Based on the Nusselt

type analysis, the following correlation is obtained for the Nusselt number, *Nu*, in the case of laminar film condensation around horizontal tubes:

$$Nu = \frac{hD_{od}}{\lambda_c} = 0.728 \left[\frac{gL\rho_c \left(\rho_c - \rho_g \right) D_{od}^{3}}{\mu_c \lambda_c \left(T_{ci} - T_{ow} \right)} \right]^{1/4} \qquad (3.12)$$

where λ_c, ρ_c and μ_c are the condensate thermal conductivity, density and molecular viscosity, respectively, and T_{ci} and T_{ow} are the temperatures at the condensate-vapor interface and tube outside wall, respectively. Undoubtedly, the most important limitation of the Nusselt analysis is that it neglects the effect of the vapor shear stress on the condensate film. This is also known as the forced convection condensation. It is expected that the vapor shear will lead to the thinning of the condensate film and thus higher heat transfer coefficients. In this study, the correlation obtained by Berman and Tumanov [36] is used to account for the effect of the vapor shear:

$$R_c' = \left(\frac{\lambda_c}{D_{od}} Nu \left(1 + 0.0095 \, \mathrm{Re}_g^{11.8/\sqrt{Nu}} \right) \right)^{-1}$$

$$\mathrm{Re}_g = \frac{\rho_g U_g D_{od}}{\mu_g} \qquad (3.13)$$

Nu in Eq. (3.13) is obtained from Eq. (3.12). Also, this relation is only valid for a single tube and the film condensation heat transfer will be very different for the flow over tube bundles than flow over a single tube. The addition of neighboring tubes adds an extra level of complexity to the problem and makes it difficult to solve. In tube bundles, the condensate from the upper tubes falls on to the lower tubes due to the gravity, which thickens the condensate film around the lower tubes. This inundation will increase the thermal resistance of the lower tubes, which needs to be considered. The relation suggested by Fuks [37] is chosen to account for the inundation effect on the heat transfer in this study:

$$\frac{R_c}{R_c'} = \left(\frac{\gamma_{tot}}{\gamma_c} \right)^n \qquad (3.14)$$

where γ_{tot} is the condensate leaving the control volume, and γ_c is condensation rate in the control volume. Different values were suggested for n in the literature. Fuks [37] took the value to be 0.07, while Grant [38] claimed that 0.223 fits the experimental data better. Later, Zhang [21] proposed a linear correlation for $n = YB$. In this method, Y is equal to 0 at the top of the tube bundle and it increases to one at the bottom, and B is a constant taken to be equal to 0.37.

The presence of even a small quantity of the non-condensable air will drastically influence the heat transfer characteristics at the liquid-vapor interface. The non-condensable air carried with the vapor accumulates at the interface between the two phases. Thus, the partial pressure of the non-condensable air at the interface gets higher than the free-stream, and the higher pressure will result in the gas diffusion away from the surface which is balanced by the vapor motion toward the surface. Also, the accumulation of the non-condensable air at the interface region decreases the vapor partial pressure and saturation temperature which is the main reason for the reduction in the heat transfer [39]. Therefore, it is important to model the thermal resistance due to the accumulation of the non-condensable gases at the gas-liquid interface. Berman and Fuks [40] obtained an empirical relation for the heat transfer characteristics of the steam-air mixture flowing in downward direction through tube bundles according to the following equation:

$$R_a = \left(\frac{aD}{D_{od}} \mathrm{Re}_g^{1/2} \left(\frac{p}{p - p_s} \right)^b p^{1/3} \left(\frac{\rho_s L}{T} \right)^{2/3} \frac{1}{(T - T_{ci})^{1/3}} \right)^{-1} \tag{3.15}$$

for $\mathrm{Re}_g > 350,$ $b = 0.6$ $\alpha = 0.52$ First Tube row

                                                    $\alpha = 0.67$ Second Tube row

                                                    $\alpha = 0.52$ Third and later Tube row

for $\mathrm{Re}_g < 350,$ $b = 0.7$ $\alpha = 0.52$

where p_s and ρ_s are the vapor partial pressure in the gas mixture and density, respectively, T and T_{ci} are the temperatures at the gas-phase free stream and interface, respectively, and D is the diffusivity of the air in the vapor.

3.2.3   Turbulence Modeling

The previous study [41] indicated that the modified RNG k-ε model gives better accuracy than other two-equation turbulence models tested. Unlike the standard RNG k-ε model, the modified RNG k-ε model takes into account the effects of the tube bundle and phase interaction drag on the turbulent kinetic energy and dissipation of the gas-phase flows and appropriate source terms are added to the k and ε equation to account for those effects. The governing equations for the modified RNG k-ε model are given as [41]:

$$\frac{\partial}{\partial t}\left(\beta_g \rho_g k\right) + \nabla \cdot \left(\beta_g \rho_g k \vec{V}_g\right) = \frac{\partial}{\partial x_j}\left[\beta_g\left(\mu_{eff}\right)\frac{\partial k}{\partial x_j}\right] - \beta_g \rho_g \varepsilon + \beta_g G_k + S_k$$

$$\frac{\partial}{\partial t}\left(\beta_g \rho_g \varepsilon\right) + \nabla \cdot \left(\beta_g \rho_g \varepsilon \vec{V}_g\right) = \frac{\partial}{\partial x_j}\left[\beta_g\left(\mu_{eff}\right)\frac{\partial \varepsilon}{\partial x_j}\right] + \beta_g C_{1\varepsilon}\frac{\varepsilon}{k}G_k - \beta_g C_{2\varepsilon}\rho\frac{\varepsilon^2}{k} - RG_\varepsilon + S_\varepsilon$$

(3.16)

where G_k is the turbulence kinetic energy generation, σ_k and σ_ε are the turbulent Prandtl numbers for k and ε, respectively, and $C_{1\varepsilon}$ and $C_{2\varepsilon}$ are constants. The term RG_ε is the source term specifically designed for the RNG model, which is the main difference between the standard k-ε model and RNG k-ε model. The extra source terms S_k and S_ε in the modified RNG k-ε model are used to account for the effects of the tube bundle and dispersed phase on the primary phase turbulence, and they are expressed as follows:

$$S_k = Rb_k + Wb_k$$
$$S_\varepsilon = Rb_\varepsilon + Wb_\varepsilon$$

(3.17)

where Rb_k and Rb_ε are the terms that account for the effect of the tube bundle on k and ε of the primary phase, respectively. Similarly, Wb_k and Wb_ε are the terms that account for the effect of the condensate droplets on k and ε, respectively. Different approaches are proposed in the literature to model these extra terms. The appropriate choice of these terms for the modified *RNG k-ε* was given in the previous work [41].

3.3 Configurations of the Condensers

Two different types of condensers are considered in this study. First, a small scale shell-and-tube experimental condenser with 400 tubes [9] is considered, as shown in Figure 3-1. The geometric and operating parameters of this condenser are given in Table 3-1. Second, an industrial full-size condenser [22] with more than 6000 tubes is selected to demonstrate the capability of the numerical method in dealing with larger, more complex industrial applications. The configuration of the full-size industrial condenser is given in Figure 3-2 and the operating conditions are provided in Table 3-2.
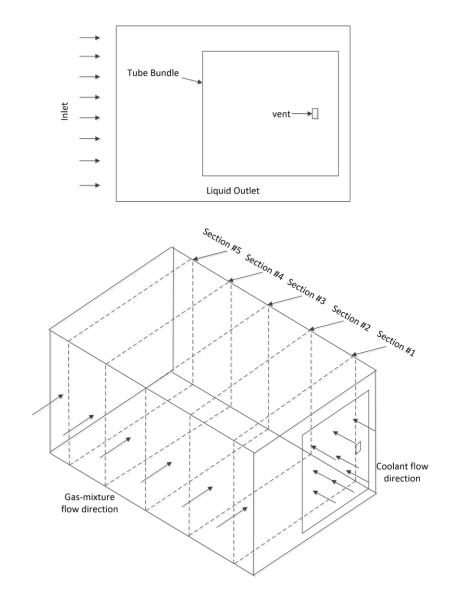
Figure 3-1: Configuration of the experimental condenser
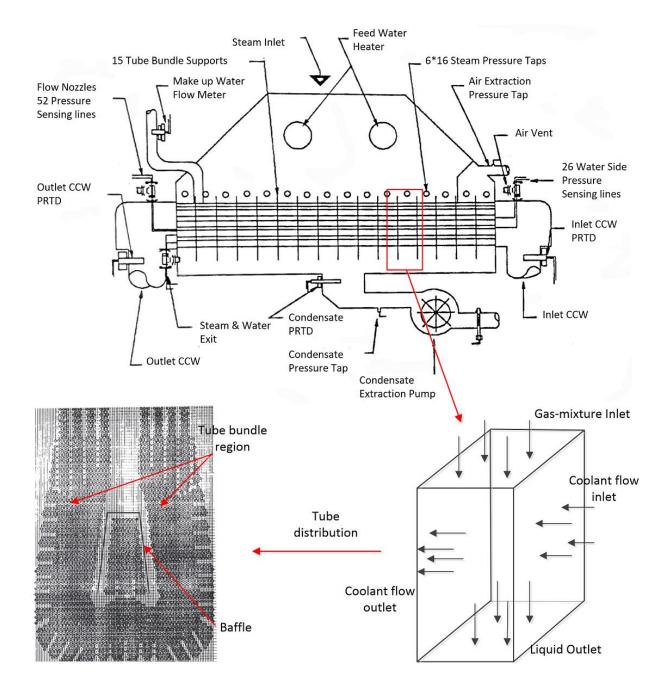
Figure 3-2: Configuration of the industrial condenser

Table 3-1: Geometric and operating parameters of the experimental condenser

Geometric parameters	
Number of tubes	400
Condenser length (m)	1.219
Condenser depth (m)	1.02
Condenser height (m)	0.78
Tube outer diameter (mm)	25.4
Tube wall thickness (mm)	1.25
Tube pitch (mm)	34.9
Operating parameters	
Inlet cooling water temperature (C)	17.8
Inlet cooling water velocity (m/s)	1.19
Inlet steam pressure (Pa)	27670
Inlet steam flow rate (kg/s)	2.032
Inlet air flow rate (Kg/s)	2.48e-04

Table 3-2: Geometric and operating parameters of the industrial condenser

Geometric parameters	
Number of tubes	6720
Condenser length (m)	17
Condenser depth (m)	2.6
Condenser height (m)	3.6
Tube outer diameter (mm)	25.4
Tube Inner thickness (mm)	22.9
Tube pitch (mm)	33.3
Operating parameters	
Inlet cooling water temperature (C)	11.58
Inlet cooling water velocity (m/s)	2.42
Total steam condensation rate (kg/s)	91.01

3.4   Solution Procedure

The quasi-three-dimensional and three-dimensional CFD simulations presented in this study are performed using ANSYS FLUENT version 14.5. First, the quasi-three-dimensional approach is used in this study. In this method, the condenser is divided into several sections along the cooling water flow direction, as shown in Figure 3-1, and the three-dimensionality effect is only considered due to the change of the cooling water temperature from one section to the next. Therefore, a two-dimensional simulation is performed in each section and the cooling water temperature is updated from one section to the next section.

In the second method, the full three-dimensional simulation is performed. The three-dimensional simulation of the shell-and-tube condensers, which is carried out in this study for the first time, includes the effect of the tube supports on the shell-side flow that was neglected in the quasi-three-dimensional approach. Moreover, the simultaneous update of the cooling water temperature is performed every iteration.

The simulations are carried out for both the small-scale experimental condenser and the full-size industrial condenser to assess the capability of the CFD model in predicting the flow and heat transfer in different type of condenser configurations.

3.4.1   Mesh

The mesh generated for both industrial and experimental condensers are created using ICEM CFD software. The structured meshes generated and used for both quasi-three-dimensional and three-dimensional approaches are presented here.

The structured two-dimensional and three-dimensional meshes for the experimental condenser are given in Figure 3-3 and Figure 3-4, respectively. There are three different zones in the computational domain. The tubular region is the only region in which condensation occurs. There is a vent in the middle of the tubular region that is used to extract non-condensable gases and the remaining steam in the condenser. In this experimental condenser, all 400 tubes are distributed uniformly with a staggered arrangement in the tube bundle region.
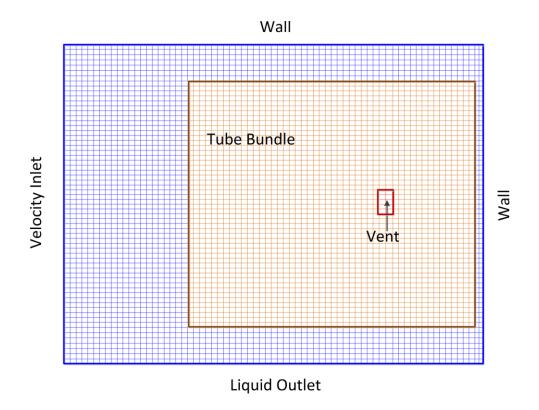
Figure 3-3: Two-dimensional mesh generated for the experimental condenser
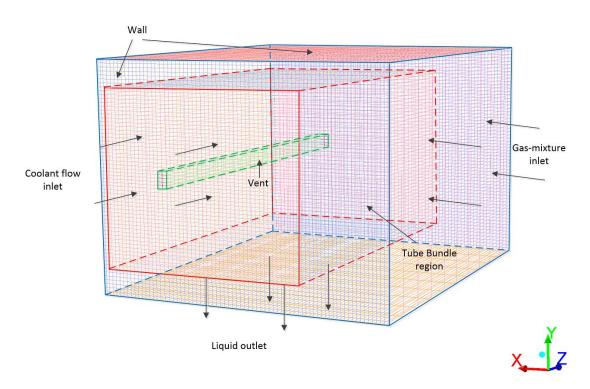
Figure 3-4: Three-dimensional mesh generated for the experimental condenser

ICEM CFD software is also used to create the structured mesh for the industrial condenser. This mesh is more complicated than that for the experimental condenser due to the presence of the baffle in the middle of the domain. Also, unlike the experimental condenser, the shape of the tube bundle of the industrial condenser is irregular. Therefore, the number of tubes in each computational cell has to be accounted for accordingly. The presence of tube supports in the industrial condenser, as shown in Figure 3-2, restricts the flow in the third direction and divides the condenser into 17 different sections. The link between different sections is through the temperature of the cooling water in the tube side. The two and three dimensional grids generated for this condenser are given in Figure 3-5 and Figure 3-6, respectively. Since there are two identical tube bundles, it is possible to use the symmetry condition to reduce the computational cost. Thus, only half of the condenser, the right side, is modeled.
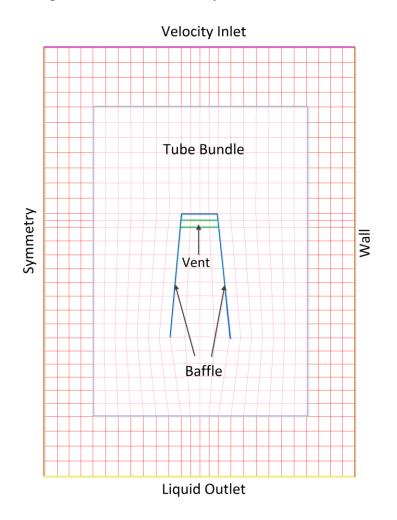
Figure 3-5: Two-dimensional mesh generated for the industrial condenser
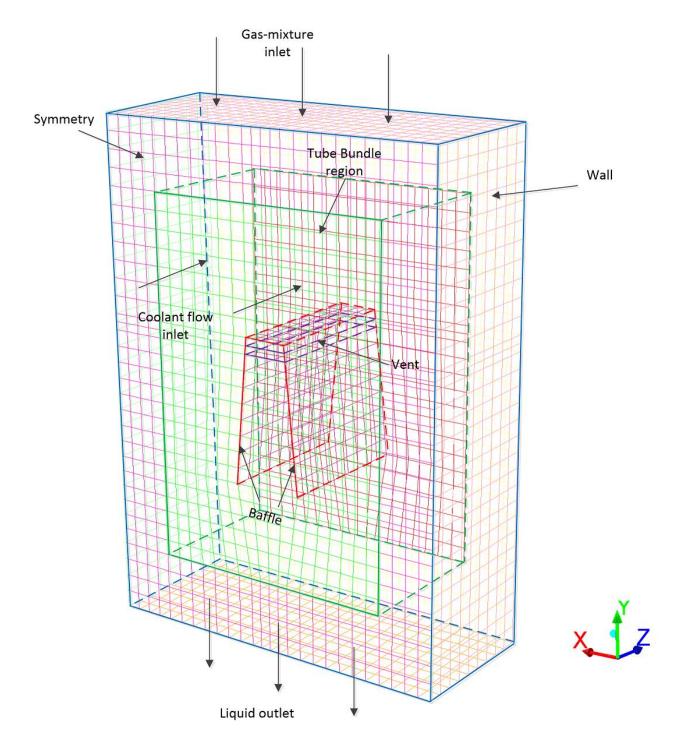
Figure 3-6: Three-dimensional mesh generated for the industrial condenser

3.4.2   Boundary Conditions

The boundary conditions for walls, outlet, inlet and vent are specified as follows and are indicated in Figure 3-3 and Figure 3-4 for the experimental condenser and Figure 3-5 and Figure 3-6 for the industrial one.

At the inlet, the velocity is considered to be uniform for each section. The velocity is not constant for all the sections, and is adjusted in an iterative process in such a way that the pressure drop from the inlet to the outlet is the same for all the sections [22]. The air mass fraction is specified at the inlet.

The bottom wall acts as an outlet for the liquid phase and as a free-slip wall for the gas-phase. This assumption means that only water can leave the domain from the bottom. This is a valid assumption since water usually leaves from the bottom of the condenser due to the gravity. This type of boundary condition is not built-in in FLUENT and requires using User Defined Functions (UDF) to specify them. The rest of the walls, including the baffle and tube supports, are specified as non-slip walls for both phases.

The vent is modeled as a mass sink, shown in Figure 3-3 and Figure 3-5. It is assumed that the amount of mass that was not condensed will leave the domain through the vent. Also, the air mass fraction at the vent is obtained accordingly.

Symmetry condition is applied to the left hand side of the domain for the industrial condenser.

3.4.3   Computational Setup

All the source terms described in Section 3.2 are implemented into FLUENT using UDF. The simulations are performed using coupled solver for the pressure–velocity coupling with very low Courant number (0.1). The first order upwind scheme is chosen for the discretization of the momentum, energy, volume fraction, turbulent kinetic energy and dissipation rate equations.

3.5   Results and Discussion

3.5.1   Experimental Condenser

To analyse the performance of the numerical method for the small-scale experimental condenser, the numerical results are compared with the experimental data by Al-Sanea et al. [9], where the average heat transfer rates between the two fluid streams at different locations in the tube bundle were reported. The comparisons of the numerical results obtained using the three-dimensional and quasi-three-dimensional approaches with the experimental data are given in Figure 3-7.
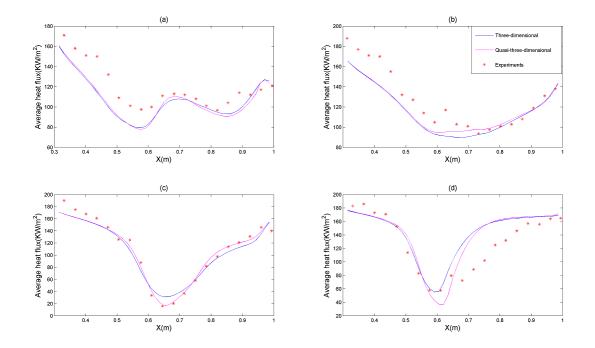
Figure 3-7: Comparison of the average heat transfer rate from the quasi-three-dimensional and three-dimensional approaches with the experimental data, (a) 3rd row tubes, (b) 8th row tubes, (c) 13th row tubes, and (d), 18th row tubes from the bottom of the tube bundle.

The comparison between the two different approaches demonstrates that there is not a significant difference between the results from the quasi-three-dimensional and three-dimensional approaches for this small-scale experimental condenser, which means the shell-side flow in the third direction is negligible. In fact, both approaches succeeded in

predicting the heat transfer rate trends in the condenser with great accuracy, about 11% difference compared to the experimental data. The three-dimensional model is more computationally expensive compared to the quasi-three-dimensional model as there are more equations and computational cells in three-dimensional case. In addition, the condensation rate contours are depicted in the Figure 3-8 for the quasi-three-dimensional and three-dimensional approaches. The condensation rate is higher at the region where the vapor enters the tubular region due to higher vapour velocity and it decreases as the vapor slows down due to condensation. The condensation rate near the vent decreases sharply due to higher concentration of the non-condensable gases near the vent. The condensation rate is very low at the bottom of tubular region due to higher liquid concentration in this region.
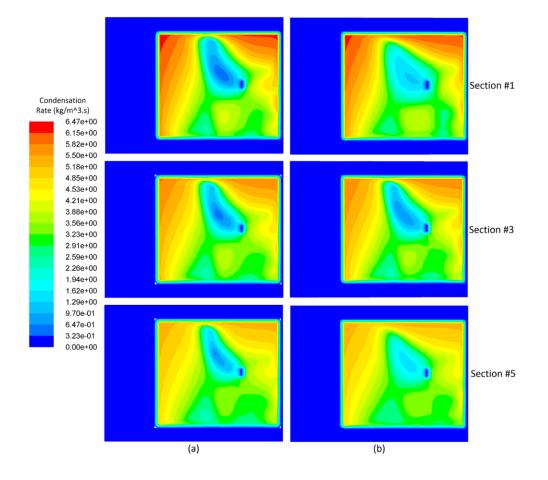
Figure 3-8: Contours of the condensation rate in the experimental condenser at different sections (a) quasi-three-dimensional approach and (b) three-dimensional approach

The inundation phenomenon can be seen from the liquid concentration distribution shown in Figure 3-9, i.e. the liquid concentration at the bottom of the tubular region is the higher than that at the top. The liquid formed around the tubes at the top region falls due to gravity on the lower tubes, which increases the thickness of the liquid film formed around them. Therefore, it is expected to see a decrease in the heat exchange between the vapor and cooling water at the bottom of the tubular region where the condensation thermal resistance is higher. This is also confirmed by the contours of the condensation rate in Figure 3-8.
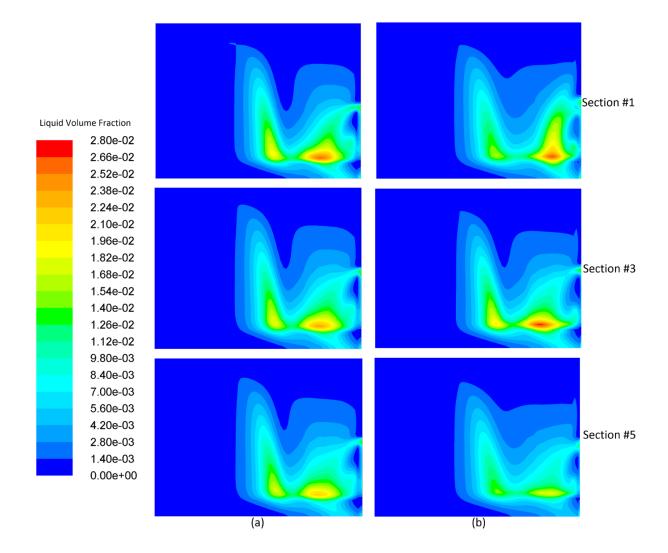
Figure 3-9: Contours of the volume fraction in the experimental condenser at different sections (a) quasi-three-dimensional approach and (b) three-dimensional approach

Moreover, it is well-known that the existence of the non-condensable gases, even small amounts, around the tube lead to a considerable reduction in the heat and mass transfer and therefore, it is important to analyze the concentration distribution of the non-condensable gases, mainly air, in the condenser. The air mass fraction contours from both quasi-three-dimensional and three-dimensional approaches are shown in Figure 3-10. The figure shows that the air is accumulated near the vent region. This accumulation is accompanied by an increase in the non-condensable gases thermal resistance and decrease in the heat and mass transfer as shown in Figure 3-8.
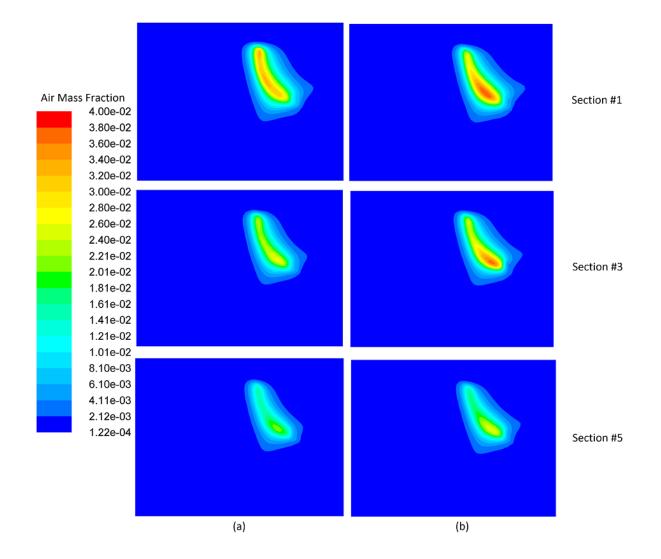
Figure 3-10: Contours of the air mass fraction in the experimental condenser at different sections (a) quasi-three-dimensional approach and (b) three-dimensional approach

3.5.2   Industrial Condenser

The experimental data given in [22] for a large-scale industrial condenser is used to test the capability of the numerical algorithm in dealing with an industrial application. This case study is a lot more challenging than the small experimental condenser as the numbers of tubes are considerably larger and the tube bundle has an irregular shape. Also there are 15 tube support plates in the condenser to support the tube bundle. The available experimental data are the pressures and temperatures at different locations on the shell side of the condenser as reported in [22]. The locations of the pressure and temperature gauges are given in Figure 3-11. The comparison of the numerically predicted pressures and temperatures from both three-dimensional and quasi-three-dimensional numerical approaches with experiments are provided in Table 3-3 and Table 3-4.
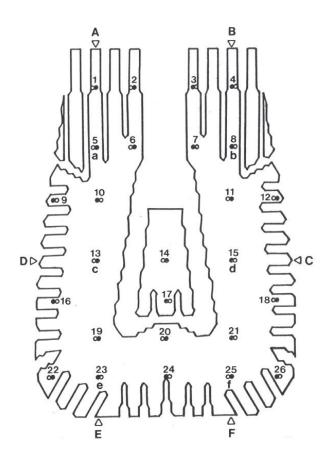
Figure 3-11: Locations of pressure gauges: A-F and temperature gauges: 5, 8, 13, 14, 15, 23, and 25 taken from [22]

Table 3-3: Comparison of the numerical results with the experimental data for the pressures in the industrial condenser

Location		A	B	C	D	E	F
Section #1	Quasi-3D	4771.94	4783.92	4643.57	4641.30	4724.61	4722.25
	% Error	3.41	4.12	5.08	0.57	4.10	4.76
	3D	4792.18	4798.97	4647.35	4662.87	4725.59	4716.64
	% Error	3.85	3.82	5.00	0.10	4.08	4.87
	Exp.	4614.40	4990.00	4892.20	4668	4926.90	4958.40
Section #2	Quasi-3D	5191.80	5201.41	5091.40	5088.93	5154.23	5152.31
	% Error	3.25	3.85	1.15	4.35	0.74	0.21
	3D	5210.21	5214.69	5094.15	5108.79	5159.69	5151.37
	% Error	3.62	3.60	1.10	4.76	0.85	0.19
	Exp.	5027.90	5409.80	5150.90	4876.40	5116.20	5141.50
Section #3	Quasi-3D	5243.73	5252.36	5154.82	5152.68	5210.35	5208.64
	% Error	1.61	2.28	1.31	4.78	1.77	0.64
	3D	5259.94	5263.83	5156.89	5170.20	5215.47	5208.09
	% Error	1.92	2.07	1.27	5.14	1.87	0.65
	Exp.	5160.40	5375.10	5223.50	4917.40	5119.40	5242.50
Section #4	Quasi-3D	5263.85	5271.59	5184.96	5183.04	5234.11	5232.61
	% Error	0.073	0.58	1.86	10.80	0.73	1.31
	3D	5278.16	5281.56	5186.47	5198.64	5238.78	5232.52
	% Error	0.19	0.39	1.83	11.14	0.82	1.31
	Exp.	5267.70	5302.50	5283.50	4677.50	5196.00	5302.50
Section #5	Quasi-3D	5214.29	5221.30	5143.29	5141.56	5187.42	5186.10
	% Error	0.12	0.70	3.17	0.66	2.05	2.42
	3D	5227.06	5230.04	5144.43	5155.62	5191.69	5186.50
	% Error	0.37	0.53	3.15	0.39	1.97	2.41
	Exp.	5207.70	5258.30	5311.90	5176.20	5296.10	5315.10
Section #6	Quasi-3D	5472.29	5478.40	5415.88	5413.29	5450.34	5449.61
	% Error	0.18	0.30	2.13	6.92	3.40	2.10
	3D	5483.13	5485.51	5416.09	5425.42	5454.60	5450.46
	% Error	0.01	0.17	2.14	7.16	3.48	2.12
	Exp.	5482.40	5495	5302.50	5062.60	5270.90	5337.20
Section #7	Quasi-3D	5381.02	5386.59	5330.78	5328.34	5361.45	5360.86
	% Error	1.30	1.69	0.12	4.34	0.45	0.84
	3D	5390.70	5392.92	5331.02	5339.18	5365.22	5361.87
	% Error	1.48	1.57	0.11	4.55	0.52	0.82
	Exp.	5311.90	5479.20	5337.20	5106.70	5337.20	5406.60
Section #8	Quasi-3D	5376.66	5381.55	5333.72	5331.34	5359.72	5359.30
	% Error	1.03	1.38	0.17	0.78	0.46	0.75
	3D	5385.04	5386.97	5333.86	5340.86	5363.03	5360.56
	% Error	1.19	1.28	0.17	0.96	0.39	0.73
	Exp.	5321.40	5457.10	5324.50	5289.90	5384.50	5400.30

Section #9	Quasi-3D	5122.93	5127.40	5083.23	5081.34	5107.24	5106.82
	% Error	1.63	1.89	0.45	0.87	1.21	3.86
	3D	5130.27	5132.10	5083.38	5089.73	5109.75	5108.07
	% Error	1.78	1.80	0.45	1.03	1.16	3.83
	Exp.	5040.50	5226.70	5106.70	5037.50	5169.90	5311.90
Section #10	Quasi-3D	5378.55	5382.16	5348.67	5346.66	5366.31	5366.09
	% Error	0.41	0.68	2.45	8.80	2.98	0.48
	3D	5384.49	5385.82	5348.55	5353.61	5368.49	5367.27
	% Error	0.53	0.61	2.45	8.94	3.02	0.50
	Exp.	5356.10	5419.20	5220.40	4914.20	5210.90	5340.30
Section #11	Quasi-3D	5338.76	5341.80	5314.25	5312.46	5328.65	5328.49
	% Error	0.50	0.73	1.00	2.01	0.07	0.28
	3D	5343.79	5344.87	5314.09	5318.40	5330.49	5329.33
	% Error	0.60	0.67	0.99	2.12	0.11	0.26
	Exp.	5311.90	5381.30	5261.50	5207.70	5324.50	5343.50
Section #12	Quasi-3D	5367.03	5369.45	5347.87	5346.31	5358.91	5358.80
	% Error	0.61	0.42	0.31	0.52	0.94	0.52
	3D	5371.08	5371.86	5347.62	5351.21	5360.49	5359.35
	% Error	0.54	0.47	0.31	0.61	0.97	0.53
	Exp.	5400.30	5346.70	5330.90	5318.30	5308.70	5330.90
Section #13	Quasi-3D	5355.54	5357.20	5340.40	5339.73	5349.24	5348.92
	% Error	1.34	1.21	0.11	4.75	2.09	0.04
	3D	5358.80	5359.38	5340.66	5343.53	5350.47	5349.59
	% Error	1.28	1.25	0.12	4.83	2.12	0.05
	Exp.	5428.70	5293	5334	5097.30	5239.30	5346.70
Section #14	Quasi-3D	5350.29	5351.63	5339.29	5338.52	5345.52	5345.35
	% Error	0.30	0.43	0.87	3.45	0.39	0.31
	3D	5352.84	5353.24	5339.31	5341.53	5346.55	5345.90
	% Error	0.35	0.40	0.87	3.50	0.41	0.30
	Exp.	5334.00	5375.10	5293	5160.40	5324.50	5362.40
Section #15	Quasi-3D	5405.98	5406.96	5398.52	5397.76	5402.56	5402.49
	% Error	0.59	0.68	0.96	3.77	1.58	2.43
	3D	5407.88	5408.14	5398.47	5400.10	5403.46	5403
	% Error	0.62	0.66	0.96	3.81	1.60	2.44
	Exp.	5374.10	5444.50	5346.70	5201.50	5318.30	5274.10
Section #16	Quasi-3D	5416.75	5417.31	5411.81	5411.43	5414.50	5414.38
	% Error	0.42	0.49	3.41	3.59	2.72	2.72
	3D	5418.12	5418.27	5411.92	5413.06	5415.19	5414.88
	% Error	0.44	0.48	3.41	3.62	2.73	2.73
	Exp.	5394	5444.50	5233.00	5223.50	5270.90	5270.90

Table 3-4: Comparison of the numerical results with the experimental data for the temperatures in the industrial condenser

Location		5	8	13	14	15	23	25
Section #1	Quasi-3D	31.137	31.18	30.775	30.431	30.794	30.935	30.959
	% Error	0.26	4.70	3.10	5.02	2.30	11.74	8.26
	3D	31.116	31.119	30.683	30.223	30.676	30.857	30.844
	% Error	0. 33	4.89	3.39	5.67	2.67	11.96	8.6
	Exp.	31.22	32.72	31.76	32.04	31.52	35.05	33.75
Section #2	Quasi-3D	32.864	32.891	32.660	32.505	32.671	32.752	32.769
	% Error	4.62	0.57	1.96	*	1.71	6.55	3.81
	3D	32.852	32.847	32.604	32.382	32.596	32.715	32.701
	% Error	4.59	0.70	1.79	*	1.48	6.66	4.01
	Exp.	31.41	33.08	32.03	*	32.12	35.05	34.07
Section #3	Quasi-3D	33.112	33.136	32.936	32.811	32.946	33.016	33.031
	% Error	*	0.49	1.74	*	3.18	6.01	2.90
	3D	33.101	33.096	32.889	32.709	32.882	32.986	32.975
	% Error	*	0.61	1.6	*	2.98	6.10	3.07
	Exp.	*	33.30	32.37	*	31.93	35.13	34.02
Section #4	Quasi-3D	33.239	33.26	33.084	32.979	33.093	33.155	33.168
	% Error	3.67	0.83	1.45	2.40	3.18	5.94	*
	3D	33.229	33.224	33.043	32.892	33.038	33.130	33.122
	% Error	3.64	0.94	1.32	2.65	3.01	6.01	*
	Exp.	32.06	33.54	32.61	33.79	32.07	35.25	*
Section #5	Quasi-3D	33.109	33.128	32.966	32.868	32.973	33.031	33.042
	% Error	2.28	2.96	*	0.76	0.25	6.61	3.80
	3D	33.100	33.096	32.929	32.794	32.924	33.009	33.003
	% Error	2.25	3.05	*	0. 98	0. 10	6.67	3.92
	Exp.	32.37	34.14	*	33.12	32.89	35.37	34.35
Section #6	Quasi-3D	34.079	34.094	33.987	33.931	33.992	34.030	34.039
	% Error	4.18	0.62	2.27	1.400	3.35	3.6599	0.78
	3D	34.071	34.067	33.959	33.873	33.955	34.015	34.010
	% Error	4.16	0.70	2.19	1.23	3.23	3.69	0.87
	Exp.	32.71	34.31	33.23	33.46	32.89	35.32	34.31
Section #7	Quasi-3D	33.805	33.819	33.720	33.670	33.724	33.759	33.767
	% Error	2.20	2.31	*	2.03	1.63	4.74	2.52
	3D	33.798	33.795	33.695	33.617	33.692	33.746	33.742
	% Error	2.201	2.38	*	1.86	1.54	4.77	2.59
	Exp.	33.07	34.62	*	33.00	33.18	35.44	34.64
Section #8	Quasi-3D	33.834	33.846	33.763	33.726	33.767	33.796	33.803
	% Error	1.20	3.10	0.34	1.89	0.24	6.40	3.08
	3D	33.827	33.825	33.742	33.682	33.740	33.785	33.782
	% Error	1.18	3.16	0.40	1.75	0.32	6.43	3.14
	Exp.	33.43	34.93	33.88	33.10	33.85	36.11	34.88

	Quasi-3D	32.973	32.984	32.895	32.856	32.899	32.931	32.937
	% Error	2.01	5.57	3.39	0.64	2.86	10.51	5.62
Section #9	3D	32.967	32.966	32.876	32.815	32.874	32.919	32.919
	% Error	2.029	5.62	3.44	0.77	2.94	10.54	5.67
	Exp.	33.65	34.93	34.05	33.07	33.87	36.80	34.90
	Quasi-3D	33.923	33.931	33.879	33.860	33.881	33.899	33.903
	% Error	0.40	*	0.50	2.60	0.05	9.28	2.12
Section #10	3D	33.917	33.916	33.864	33.831	33.863	33.889	33.891
	% Error	0.41	*	0.54	2.51	0.10	9.31	2.16
	Exp.	34.06	*	34.05	33	33.90	37.37	34.64
	Quasi-3D	33.822	33.828	33.788	33.775	33.790	33.804	33.807
	% Error	0.11	4.06	1.52	2.13	1.83	10.45	3.68
Section #11	3D	33.817	33.816	33.776	33.752	33.775	33.795	33.798
	% Error	0.12	4.09	1.55	2.06	1.87	10.47	3.70
	Exp.	33.86	35.26	34.31	33.07	34.42	37.75	35.10
	Quasi-3D	33.953	33.958	33.930	33.922	33.932	33.941	33.944
	% Error	1.06	4.42	1.65	2.35	2.91	12.52	3.81
Section #12	3D	33.949	33.948	33.920	33.905	33.919	33.933	33.936
	% Error	1.08	4.45	1.68	2.30	2.94	12.54	3.83
	Exp.	34.32	35.53	34.50	33.14	34.95	38.80	35.29
	Quasi-3D	33.944	33.947	33.929	33.924	33.930	33.936	33.938
	% Error	1.38	4.50	1.93	2.80	2.72	10.71	1.88
Section #13	3D	33.941	33.940	33.921	33.911	33.921	33.930	33.932
	% Error	1.39	4.52	1.96	2.76	2.74	10.73	1.90
	Exp.	34.42	35.55	34.60	33.00	34.88	38.01	34.59
	Quasi-3D	33.953	33.955	33.944	33.941	33.944	33.949	33.95
	% Error	1.47	3.78	6.59	2.54	3.86	10.06	3.19
Section #14	3D	33.95	33.94	33.93	33.93	33.93	33.94	33.94
	% Error	1.47	3.79	6.60	2.51	3.88	10.08	3.20
	Exp.	34.46	35.29	36.34	33.10	35.31	37.75	35.07
	Quasi-3D	34.164	34.165	34.159	34.158	34.160	34.162	34.163
	% Error	1.43	2.41	5.61	3.28	4.47	9.57	3.38
Section #15	3D	34.161	34.161	34.155	34.152	34.155	34.158	34.159
	% Error	1.43	2.42	5.62	3.27	4.48	9.58	3.39
	Exp.	34.66	35.01	36.19	33.07	35.76	37.78	35.36
	Quasi-3D	34.218	34.218	34.216	34.216	34.216	34.218	34.218
	% Error	1.38	1.84	5.58	1.80	6.02	8.13	3.61
Section #16	3D	34.216	34.216	34.213	34.211	34.213	34.215	34.216
	% Error	1.39	1.84	5.59	1.78	6.03	8.14	3.61
	Exp.	34.70	34.86	36.24	33.61	36.41	37.25	35.50

Similar to the case of the experimental condenser, the three-dimensional approach does not provide a significant improvement over the quasi-three-dimensional approach since the support plates in the industrial condenser restricts the shell-side flow in the third

direction. Nonetheless, both approaches succeeded in predicting the steam pressure and temperature with a great accuracy; the average error for the prediction of the steam pressures is 1.8% and for the steam temperatures is 3.2 %, which is 28% and 25% percent improvement for the pressure and temperature predictions with respect to the previous analysis conducted by Zhang [22]. In the study by Zhang [22], a single phase CFD model was used with a constant viscosity approach.

The condensation rate contours are depicted in Figure 3-12. Unlike the experimental condenser where the tube bundle has a rectangular shape, the tube bundle in the industrial condenser has an irregular shape. The condensation rate depends on the number of tubes. In the industrial condenser, there are more tubes in the bottom of the tube bundle than the top. Therefore, as it can be seen from Figure 3-12, the condensation rate is higher at the bottom of the tube bundle than the top although the inundation has stronger effect for the heat transfer in the bottom of the tube bundle than the top. In addition, the vapor velocity is high at the bottom of the tube bundle, which also enhances the heat transfer in the bottom region. The velocity vectors for the gas and liquid phases are given in Figure 3-13.

Figure 3-12: Contours of the condensation rate in the industrial condenser (Section #1) (a) quasi-three-dimensional approach and (b) three-dimensional approach
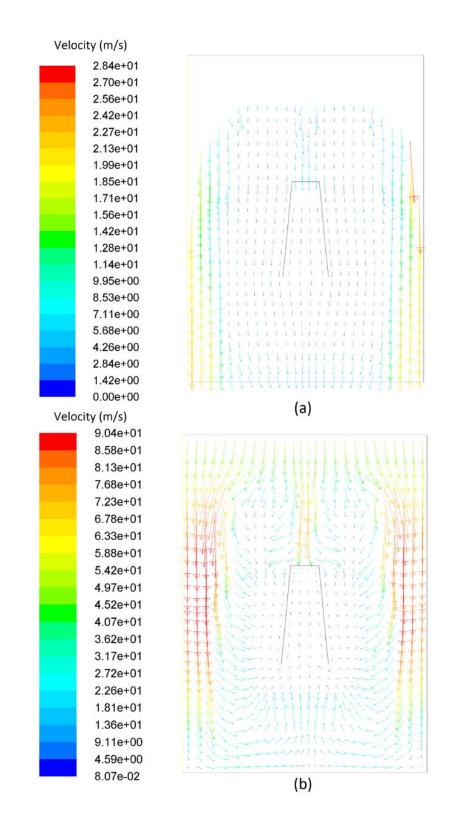
Figure 3-13: Velocity vectors (Section #1) (a) liquid phase and (b) gas phase

The condensation rate is at its lowest inside the baffle region as shown in Figure 3-12. There are two reasons for this phenomenon. First, the vapor-gas mixture velocity is at its lowest inside the baffle region due to the condensation and therefore, heat transfer rate is decreased between the shell and tube-sides. Second, the non-condensable gases, mainly air in this case, accumulate near the vent region where they are being extracted from the condenser, as shown in Figure 3-14. This increase in the concentration of the air will lead to an increase in the total thermal resistance, which results in a decrease in the heat transfer and condensation rates.
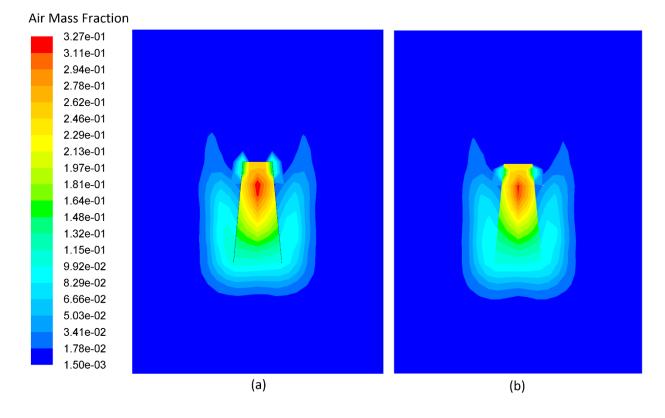
Figure 3-14: Contours of the air mass fraction for the industrial condenser (Section #1) (a) quasi-three-dimensional approach and (b) three-dimensional approach

The volume fraction of the liquid phase or condensate is shown in Figure 3-15. The inundation phenomenon or the accumulation of the condensate liquid at the bottom of tubular region is clearly visible in this figure.
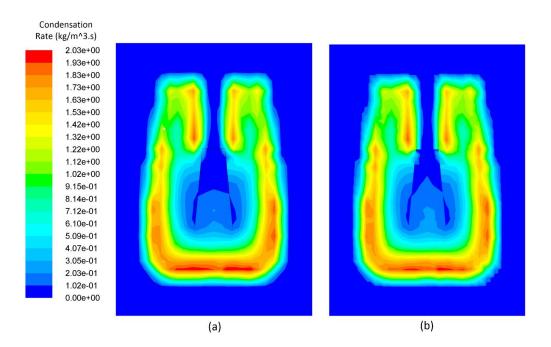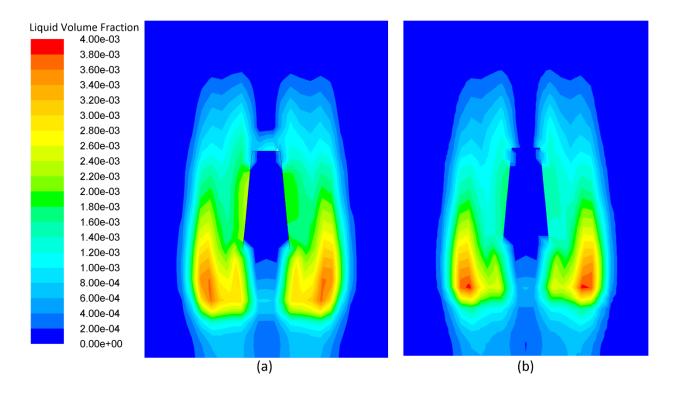

Figure 3-15: Contours of the liquid volume fraction for the industrial condenser (Section #1) (a) quasi-three-dimensional approach and (b) three-dimensional approach

3.6   Conclusions

A comprehensive numerical model was proposed to analyze the fluid flow and heat transfer in small and large scale condensers. The Eulerian-Eulerian two-phase model was chosen for this study and separate conservation equations for the liquid and gas phases were solved. The interphase interaction between the two phases was modeled by considering the interface drag, and heat and mass transfer due to the condensation. The tubular region was treated as a porous media to avoid the problem of solving the detailed flow and temperature fields around each tube in the condenser. Also a modified RNG k-ε

turbulence model from the previous work was used to account for the turbulence effects on the fluid flow and heat transfer in condensers. The effects of the non-condensable gases and condensate inundation on the heat and mass transfer were also considered by including the corresponding thermal resistances.

Both quasi-three-dimensional and three-dimensional approaches were adopted in this study to account for the three-dimensional effects. The simulations were carried out for a small-scale experimental condenser and a full-size industrial condenser. For the first time a comprehensive three-dimensional two-phase CFD model was proposed to solve the turbulent flow and heat transfer in a full-scale industrial condenser with an irregular shape. It was shown that the numerical method is capable of accurately predicting the heat and mass transfer rate as well as the pressure and temperature. This model can be easily implemented in commercial software and can be used for a wide range of condenser configurations.

It was found that the three-dimensional approach does not provide a significant improvement over the quasi-three-dimensional approach, and both methods are able to predict the performance of condensers with a considerable accuracy. However, the three-dimensional approach eliminates the need to perform separate two dimensional analysis for each section and transferring data between each computational section by updating the coolant water temperature at each iteration.

.

References

[1]   P. O'Kelly, *Computer Simulation of Thermal Plant Operations*: Springer, 2012.

[2]   Y. He, W. Tao, B. Deng, X. Li, and Y. Wu, "Numerical simulation and experimental study of flow and heat transfer characteristics of shell side fluid in shell-and-tube heat exchangers," in *Proceedings of Fifth International Conference on Enhanced, Compact and Ultra-Compact Heat Exchangers: Science, Engineering and Technology, Hoboken, NJ, USA*, 2005, pp. 29-42.

[3]   I. S. Ramón and M. P. González, "Numerical study of the performance of a church window tube bundle condenser," *International journal of thermal sciences,* vol. 40, pp. 195-204, 2001.

[4]   H. Zeng, J. a. Meng, and Z. Li, "Numerical study of a power plant condenser tube arrangement," *Applied Thermal Engineering,* vol. 40, pp. 294-303, 2012.

[5]   S. Kakac, H. Liu, and A. Pramuanjaroenkij, *Heat exchangers: selection, rating, and thermal design*: CRC press, 2012.

[6]   M. Prithiviraj and M. J. Andrews, "Three dimensional numerical simulation of shell-and-tube heat exchangers. Part I: foundation and fluid mechanics," *Numerical Heat Transfer, Part A: Applications,* vol. 33, pp. 799-816, 1998.

[7]   S. Patankar and D. Spalding, "Heat exchanger design theory source book," *Scripta Book Co., Washington, DC,* pp. 155-176, 1974.

[8]   B. Davidson and M. Rowe, "Simulation of power plant condenser performance by computational methods: an overview," *Power Condenser Heat Transfer Technology,* pp. 17-49, 1981.

[9]   S. Al-Sanea, N. Rhodes, D. Tatchell, and T. Wilkinson, "A computer model for detailed calculation of the flow in power station condensers," in *Condensers: theory and practice. Symposium*, 1983, pp. 70-88.

[10]   S. Al-Sanea, N. Rhodes, and T. Wilkinson, "Mathematical modelling of two-phase condenser flows," in *Proceedings of the BHRA 2nd International Conference on Multi-Phase Flow, London*, 1985, pp. 169-182.

[11]   T. Rabas and A. Kassem, "The Effect of Equal Shellside Pressure Drops on the Thermal Performance of Single-Pass,'X'-Shell, Steam Condensers," in *23rd ASME-AIChE National Heat Transfer Conference, Denver, Colorado*, 1985.

[12]   J. McNaught and C. Cotchin, "Heat transfer and pressure drop in a shell and tube condenser with plain and low-fin tube bundles," *Chemical engineering research & design,* vol. 67, pp. 127-133, 1989.

[13]   A. Bush, G. Marshall, and T. Wilkinson, "The prediction of steam condensation using a three component solution algorithm," in *Proceedings of the Second International Symposium on Condensers and Condensation, University of Bath, UK*, 1990, pp. 223-234.

[14]   M. R. Malin, "Modelling flow in an experimental marine condenser," *International Communications in Heat and Mass Transfer,* vol. 24, pp. 597-608, 1997.

[15]   R. Roy, V. Gokhale, and M. Ratisher, "A computational model of a power plant steam condenser," *Journal of energy resources technology,* vol. 123, pp. 81-91, 2001.

[16]   M. Prieto, I. Suarez, and E. Montanes, "Analysis of the thermal performance of a church window steam condenser for different operational conditions using three models," *Applied thermal engineering,* vol. 23, pp. 163-178, 2003.

[17]   S. Ormiston, G. Raithby, and L. Carlucci, "Numerical modeling of power station steam condensers—Part 1: Convergence behavior of a finite-volume model," *Numerical Heat Transfer,* vol. 27, pp. 81-102, 1995.

[18]   S. Ormiston, G. Raithby, and L. Carlucci, "Numerical modeling of power station steam condensers—Part 2: Improvement of solution behavior," *Numerical Heat Transfer,* vol. 27, pp. 103-125, 1995.

[19]   H. G. Hu and C. Zhang, "A modified k–ε turbulence model for the simulation of two-phase flow and heat transfer in condensers," *International Journal of Heat and Mass Transfer,* vol. 50, pp. 1641-1648, 2007.

[20]   H. G. Hu and C. Zhang, "Evaluations of closure correlations for the simulation of two-phase flows in condensers," *Heat Transfer Engineering,* vol. 30, pp. 437-451, 2009.

[21]   H. G. Hu and C. Zhang, "A new inundation correlation for the prediction of heat transfer in steam condensers," *Numerical Heat Transfer, Part A: Applications,* vol. 54, pp. 34-46, 2008.

[22]   C. Zhang, "Numerical modeling using a quasi-three-dimensional procedure for large power plant condensers," *Journal of heat transfer,* vol. 116, pp. 180-188, 1994.

[23]   C. Zhang, "Local and overall condensation heat transfer behavior in horizontal tube bundles," *Heat transfer engineering,* vol. 17, pp. 9-30, 1996.

[24]   C. Zhang and A. Bokil, "A quasi-three-dimensional approach to simulate the two-phase fluid flow and heat transfer in condensers," *International journal of heat and mass transfer,* vol. 40, pp. 3537-3546, 1997.

[25]   C. Zhang, A. Sousa, and J. Venart, "The numerical and experimental study of a power plant condenser," *Journal of heat transfer,* vol. 115, pp. 435-445, 1993.

[26]   C. Zhang, A. Sousa, and J. Venart, "Numerical simulation of different types of steam surface condensers," *Journal of Energy Resources Technology,* vol. 113, pp. 63-70, 1991.

[27]   C. Zhang and Y. Zhang, "A quasi-three-dimensional approach to predict the performance of steam surface condensers," *Journal of energy resources technology,* vol. 115, pp. 213-220, 1993.

[28]   C. Zhang and Y. Zhang, "Sensitivity analysis of heat transfer coefficient correlations on the predictions of steam surface condensers," *Heat transfer engineering,* vol. 15, pp. 54-63, 1994.

[29]   I. Nedelkovski, I. Vilos, and T. Geramitcioski, "Finite element solution of Navier-Stokes equations for steam flow and heat transfer," *Momentum,* vol. 1000, p. 1, 2005.

[30]   A. Rusowicz, "The numerical modeling and measurements for power plant condenser," 2009.

[31]   D. Rhodes and L. Carlucci, *Predicted and measured velocity distributions in a model heat exchanger*: Chalk River Nuclear Laboratories, 1984.

[32]   R. Clift, J. R. Grace, and M. E. Weber, *Bubbles, drops, and particles*: Courier Dover Publications, 2005.

[33]   F. P. Incropera, A. S. Lavine, and D. P. DeWitt, *Fundamentals of heat and mass transfer*: John Wiley & Sons, 2011.

[34]   V. Gnielinski, "New equations for heat and mass transfer in the turbulent flow in pipes and channels," *NASA STI/Recon Technical Report A,* vol. 75, p. 22028, 1975.

[35]   W. Nusselt, "The condensation of steam on cooled surfaces," *Z. Ver. Dtsch. Ing,* vol. 60, pp. 541-546, 1916.

[36]   D. Chisholm, "Modern developments in marine condensers: Noncondensable gases: An overview," *Power Condenser Heat Transfer Technology,* pp. 95-142, 1981.

[37]   S. N. Fuks, "Heat transfer with condensation of steam flowing in a horizontal tube bundle," *Teploenergetika,* vol. 4, pp. 35-39, 1957.

[38]   I. D. R. Grant and B. D. J. Osment, *The Effect of Condensate Drainage on Condensor Performance*: National Engineering Laboratory, 1968.

[39]   J. G. Collier and J. R. Thome, *Convective boiling and condensation*: Oxford University Press, 1994.

[40]   S. M. Ghiaasiaan, *Two-Phase Flow, Boiling, and Condensation: In Conventional and Miniature Systems*: Cambridge University Press, 2008.

[41]   P. Mirzabeygi and C. Zhang, " Turbulence modeling for two phase flow and heat transfer in condensers," Submitted to International Journal of Multiphase Flow|.

Chapter 4

4 Multi-objective optimization of a steam surface condenser using Territorial Particle Swarm technique

4.1 Introduction

Condensers are vital components of every power plant, and any improvement which leads to an increase in the efficiency will in turn increase the power generation and lower the operational costs of the unit. Indeed, lowering the cost of the power generation has a significant value in today's world with ever-increasing demands for energy and electricity.

However, it is not a straightforward task to provide an efficient, compact and economical design for power plant condensers. The traditional methods of condenser designs were mostly based on the experience, previous designs and experimental data [1-4]. However, a more thorough knowledge of the flow and heat transfer inside condensers is necessary to improve the condenser design. This knowledge can come from either experiments or computational analysis, but experimental analysis is usually very costly and time consuming. Also, it is very difficult to extract detailed information such as turbulence measurements through this method of analysis [5]. Therefore, this leaves us with the other option that is using numerical methods to obtain the comprehensive knowledge about the fluid flow and heat transfer inside condensers in order to provide better design solutions.

Numerical studies of condensers have been conducted by several researchers [6-26]. The first numerical model was developed by Al-Sanea et al. [8], in which they included the interphase effect in their two-phase model. Rabas and Kassem [9] studied the effect of the condensate inundation and neglected the vapor shear effect on the convective heat transfer in condensers. McNaught and Cotchin [10] implemented a new correlation to account for the effect of the inundation. Bush et al. [11] predicted the flow and heat transfer in an experimental condenser using a two-phase model. Moreover, Zhang and Bokil [22] included the interphase effect and used a two-phase model to simulate a

condenser. Hu and Zhang [17] developed a modified k-ε turbulence model for the two-phase flow in condensers and, later assessed the effects of different closure correlations on the numerical simulations [18] and proposed a new correlation to account for the effect of the inundation on the condensation heat transfer in condensers [19].

There are some researches devoted to heat exchanger optimizations which are discussed here. Selbas et al. [27] used a logarithmic mean temperature difference (LMTD) method and a genetic optimization method to find the optimal design of shell-and-tube heat exchangers. Ponce-Ortega et al. [28] used Bell-Delaware [29] method in combination with a genetic algorithm to find the optimized design of a shell-and-tube condenser. Later, Fesanghary et al. [30] used the global sensitivity analysis (GSA) and harmony search algorithm (HSA) for the design optimization of shell-and-tube heat exchangers from the economic viewpoint. They used Bell-Delaware method to obtain the average shell-side heat transfer coefficient. Patel and Rao [31] solved a cost minimization using Particle Swarm Optimization (PSO) technique and LMTD method. Zeng et al. [3] studied three conventional tube configurations and proposed a new tube configuration based on the analysis.

Surprisingly, there has never been a research focusing on the application of the CFD analysis of condensers for the condenser design optimization. The researchers who proposed CFD models for detailed condenser analysis never used their CFD models as a tool to improve the condenser designs using a systematic optimization procedure. Similarly, the researchers who studied the heat exchanger design optimization only used simple approaches to obtain the fluid flow, and heat and mass transfer information in the condenser. Therefore, the aim of this paper is to fill this gap by developing a procedure using more accurate numerical simulation results in combination with a robust optimization algorithm to optimize the condenser design.

The Eulerian-Eulerian two-phase model is used for the simulations of the fluid flow and heat transfer in condensers. The conservation equations are solved for both liquid and gas phases and the effect of condensation, interphase drag, and flow resistance due to the presence of tubes are added as source terms to the corresponding conservation equations

according to the previous work [32]. Turbulence effects are considered by solving a turbulence model for the gas-phase (the primary phase) as suggested in the previous work [33]. Also it is well known that even a small amount of non-condensable gases presented around the tubes would lead to a considerable reduction in the heat transfer rate and steam condensation rate. Species transport equation is solved to track the accumulation of non-condensable gases in the condenser. This two- phase model is capable of assessing the condenser performance [32].

A modified Multi-Objective PSO (MOPSO) algorithm with a territorial diversity-preserving scheme, named Multi-Objective Territorial Particle Swarm Optimization (MOTPSO) [34], is chosen for the optimization of condenser designs in this study. The MOPSO algorithm is a multi-objective version of the original PSO algorithm that is a Swarm Intelligence technique developed by Kennedy et al. [35] inspired by the social behavior among animals like birds and fishes. The reason behind this choice is that the MOTPSO algorithm improves the exploitation and exploration capabilities of the original PSO algorithm. The MOPSO has been modified using two different approaches. The first approach uses a spatial territory for each particle to avoid the problem of the premature convergence around a local optimum without through search of the entire domain. This modification, indeed, enhances the exploratory behavior in MOPSO. In the second approach, a new direction is introduced which moves the particle towards a new position, instead of its own best experienced position. This particular type of interaction precludes the quick spread of the information among particles, moves the particle toward a candidate region in its neighborhood, and encourages exploitation of the nearest found so far in the local optimum. Thus, it enhances the exploitative behavior of the MOPSO. This algorithm is shown to perform better than other state-of-the art swarm intelligence techniques and evolutionary algorithms on several single and multi-objective benchmark functions [34, 36].

This chapter is organized as follows: Section 4.2 provides a description of the optimization algorithm used in this study. Next, the theory of fluid flow, heat and mass transfer in a shell-and-tube condenser is discussed in Section 4.3 and the governing equations and auxiliary relations are presented in this section. The numerical setup and

objective functions are introduced in Section 4.4. The geometry and operating parameters, mesh generation, boundary conditions and optimization procedure are all discussed in this section. In Section 4.5, the optimization results are presented and discussed. Finally, conclusion and future work are given in Section 4.6.

4.2   Multi-Objective Territorial Particle Swarm Optimization (MOTPSO)

In the original PSO algorithm [35], a "swarm" of particles representing potential solutions move in the N-dimensional space of design variables. The fitness of each particle is a function of its position vector **X**. This position is updated in each time step as the particle flies around the design space in search for potential good candidates. The movement of the particle is represented by the velocity vector **Vp**. In the PSO algorithm, the particle has memory and remembers its own best position (personal leader) **P** and the swarm's best position (global leader) **G** found so far. It is really important to notice that the particles in the PSO algorithm only represent a candidate configuration in the design space, and their position and velocity does not have a physical significance in the CFD simulation.

In each time step t, the velocity is updated and the particle is moved to a new position. The new position is determined by the sum of the previous position and the new velocity according to

$$\mathbf{X}^{t+1} = \mathbf{X}^t + \mathbf{V}p^{t+1} \tag{4.1}$$

The new velocity is obtained using the previous velocity, position and individual and social memories

$$\mathbf{V}p^{t+1} = W \cdot \mathbf{V}p^t + \phi_1 \cdot \left(\mathbf{P}^t - \mathbf{X}^t\right) + \phi_2 \cdot \left(\mathbf{G}^t - \mathbf{X}^t\right) \tag{4.2}$$

where ϕ_1 and ϕ_2 are real numbers chosen uniformly and randomly in some interval, usually [0, 2] and used to determine the significance of **P** and **G** in the calculation of the

new velocity. The inertia weight W weighs the magnitude of the old velocity $\mathbf{Vp^t}$ in the calculation of the updated velocity $\mathbf{Vp^{t+1}}$. The superscript represents the time step t.

To explain how MOTPSO algorithm improves upon the original PSO, it is important to understand the processes of choosing the personal and global leaders for each particle in the swarm using the single and multi-objective optimization methods are completely different. First, in the single-objective method, the leader is globally determined for the whole swarm, however, in the multi-objective method, there is a set of non-dominated solutions, called the external archive where each particle chooses its leader from and updates its position. Therefore, an archive is created to store the non-dominated solutions found so far by the particles. This storage place is separated from the original swarm and the solutions in this archive are selected to be the leaders for individual particles in the swarm. A leader is selected for each particle from the external archive. A quality criterion is used to select a leader for each particle from the archive. This criterion, which is called the nearest neighbor density estimator [37], indicates how crowded is the closest neighbors of a given particle in the objective function space. Then the particles in the less crowded regions are more likely to be selected as leaders, see Figure 4-1.
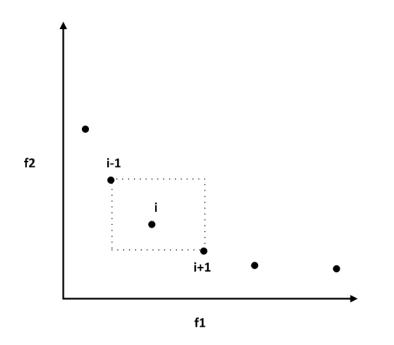

Figure 4-1: Nearest neighbor density estimator quality criterion for the leader selection from the archive [34]

Then, the concept of the personal leader or the personal best memory P needs to be modified in the transition from the single-objective to multi-objective algorithm. A particle's new position replaces its current personal best if the personal best is being dominated by the particle's new position or they are non-dominated with respect to each other. The global best, personal best and external archive concepts for minimizing two objectives are demonstrated in Figure 4-2.
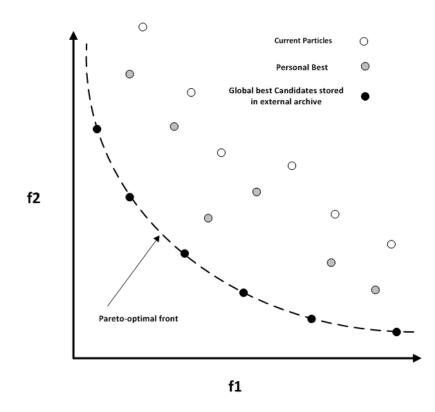
Figure 4-2: Global best, personal best and external archive concepts for two minimum objectives [34]

In the MOTPSO method [34, 36], several modifications have been made to improve the performance of the original PSO algorithm in both single and multi-objective modes. The modified velocity update equation is given as:

$$\mathbf{V}p_i^{t+1} = \chi \times \left(\mathbf{W} \times \mathbf{V}p_i^t + \phi_1 \left(\mathbf{P}_i^{*t} - \mathbf{X}_i^t \right) + \phi_2 \left(\mathbf{G}_i^t - \mathbf{X}_i^t \right) \right) + \phi_3 \sum_j Collision_i^j \qquad (4.3)$$

A constriction coefficient χ, as suggested by Nejat and Mirzabeygi [34], is used to limit the maximum velocity.

$$\chi = \frac{2}{2 - \varphi - \sqrt{\varphi^2 - 4\varphi}} \tag{4.4}$$

where φ is obtained as follows:

$$\varphi = \begin{cases} \phi_1 + \phi_2 & \text{if } \phi_1 + \phi_2 > 4 \\ 1 & \text{if } \phi_1 + \phi_2 \leq 4 \end{cases} \tag{4.5}$$

Moreover, the MOTPSO algorithm has two main mechanisms to enhance the exploratory and exploitative ability of the original algorithm and keep the balance between these two [34, 36]. First, to prevent the particles from clustering around a local optimum found prematurely at the beginning of the search process, a territory is defined around each particle. When an intruder particle enters this space, a collision operator shown below will act upon both host and intruder particles.

$$Collision_i^j = \begin{cases} \left(2Ra^t - \|\mathbf{X}_i - \mathbf{X}_j\|\right) \dfrac{\mathbf{X}_i - \mathbf{X}_j}{\|\mathbf{X}_i - \mathbf{X}_j\|} & F_j \text{ dominates } F_i \\ 0 & \text{else} \end{cases} \tag{4.6}$$

The weaker particle (the particle that is being dominated by the other particle) will be sent back to the distance $2Ra$. In Eq.(4.6), the term F_i is the fitness of the host particle and F_j is the fitness of the intruder particle in the territory. The territory of each particle has spherical shape in the N-dimensional space with the initial radius given as follows:

$$Ra_{max} = \frac{\sqrt[N]{\left(\prod_{i=1}^{N}\left(X_U^i - X_L^i\right)\right)} \Big/ K}{4} \tag{4.7}$$

In the above equation, N is the number of variables or dimensions, K is the swarm size, and X^i_U and X^i_L are the upper and lower bounds of ith variable or dimension, respectively. However, maintaining this large territory radius throughout the whole search process prevents the particles to converge to a final solution, therefore, the territory size of each particle is to decrease to zero in a linear fashion.

In the second mechanism, the MOTPSO method moves the particle to a new direction which is a weighted average of the best found positions of its elite neighbors so far, instead of attracting each particle towards its own best position. This new position, that is called P^*, is the replacement for P in the original algorithm, and represents a local optimum candidate near the particle [36]. The inverse square of the distance between the particle and its neighbors is taken to be the weight to find the average. Note that, for a given particle i only the "elite" neighbors contribute to determine the direction. "Elite" neighbors mean the neighbor particles that their best found positions so far, P_j, dominate the current particle's position, F_i. The new position P^* is defined according to the following equation.

$$\mathbf{P}^*_i = \frac{\displaystyle\sum_{j\left(P_j \text{ dominate } F_i\right)} \mathbf{P}_j \frac{1}{\left\|\mathbf{X}_i - \mathbf{P}_j\right\|^2}}{\displaystyle\sum_{j\left(P_j \text{ dominate } F_i\right)} \frac{1}{\left\|\mathbf{X}_i - \mathbf{P}_j\right\|^2}} \tag{4.8}$$

A polynomial mutation operator [38] was chosen and it was applied for 15% of the swarm particles to further enhance the diversity of the final solution.

$$\mathbf{X}_j\left(t+1\right) = \mathbf{X}_j\left(t\right) + \left(\mathbf{X}^j_U - \mathbf{X}^j_L\right) \times \delta_j \tag{4.9}$$

The terms X^j_U and X^j_L represent upper and lower bounds of the design variable, and δj is calculated from a polynomial probability distribution, and is defined as follows:

$$\delta_j = \begin{cases} \left(2r_j\right)^{1/(\eta+1)} - 1 & r_j < 0.5 \\ 1 - 2\left(1 - r_j\right)^{1/(\eta+1)} & r_j \geq 0.5 \end{cases} \tag{4.10}$$

The parameter rj is a random number between 0 and 1, and η is the polynomial distribution index which is used to tune the degree of perturbation.

Here is the summary on how the optimization algorithm works: (1) the swarm is initialized, (2) the external archive is also initialized with the non-dominated particles from the swarm, (3) the nearest neighbor density estimator quality is calculated for all the

leaders in order to select a leader Gi for each particle of the swarm, (4) the P* is calculated for each particle according to Eq. (4.8), (5) knowing these two values, the velocity is updated, the flight is performed for each particle, and the polynomial mutation operator is performed after the flight, (6) the particle's fitness is evaluated, and its corresponding P and the set of leaders are updated, and (7) the quality measure of the leaders is recalculated. This process is repeated for a certain number of iterations.

4.3 CFD Models

The Eulerian-Eulerian multi-phase phase CFD model is used to solve the two-phase flow and heat transfer in the condenser. In this approach, the fluids of both phases are assumed to behave as continuous media and a set of conservation equations is solved for each phase. The mass conservation equations are given as:

$$\frac{\partial}{\partial t}\left(\beta_g \rho_g\right) + \nabla \cdot \left(\beta_g \rho_g \vec{V}_g\right) = -S_{mass}$$

$$\frac{\partial}{\partial t}\left(\beta_l \rho_l\right) + \nabla \cdot \left(\beta_l \rho_l \vec{V}_l\right) = S_{mass}$$

$$S_{mass} = \dot{m}$$

$$\beta_g + \beta_l = \alpha$$

(4.11)

The Eulerian-Eulerian multi-phase phase CFD model is used to solve the two-phase flow and heat transfer in the condenser. In this approach, the fluids of both phases are assumed to behave as continuous media and a set of conservation equations is solved for each phase. The mass conservation equations are given as:

$$\frac{\partial}{\partial t}\left(\beta_g \rho_g\right) + \nabla \cdot \left(\beta_g \rho_g \vec{V}_g\right) = -S_{mass}$$

$$\frac{\partial}{\partial t}\left(\beta_l \rho_l\right) + \nabla \cdot \left(\beta_l \rho_l \vec{V}_l\right) = S_{mass}$$

$$S_{mass} = \dot{m}$$

$$\beta_g + \beta_l = \alpha$$

(4.12)

where the mass condensation rate $\dot{m}$ is added as the sink and source terms to the gas-phase and liquid-phase continuity equations, respectively. In Eq. (4.11), β_g and β_l are the

gas and liquid volume fractions and they represent the volume of fluid occupied by the gas and liquid, respectively. The term α is the porosity, which is defined as the ratio of the volume occupied by the fluid to the total volume. The porous media approach is used in this study to account for the effect of the presence of the tube bundle on the fluid flow in the condenser. This approach does not need the detailed analysis of the fluid flow, and heat and mass transfer around each tube and models the tube bundle as the distributed flow resistance against the shell-side flow. The porosity, α, is given as follows for the tube bundle with a staggered arrangement:

$$\begin{cases} \alpha = 1 & \text{For non-tube bundle region} \\ \alpha = 1 - \dfrac{\pi}{2\sqrt{3}}\left(\dfrac{D_{od}}{P_t}\right)^2 & \text{For tube bundle region} \end{cases} \tag{4.13}$$

The terms D_{od} and P_t represent the tube outer diameter and pitch, respectively. The momentum conservation equations for both phases are given as:

$$\begin{aligned} &\frac{\partial}{\partial t}\left(\beta_g \rho_g \vec{V}_g\right) + \nabla \cdot \left(\beta_g \rho_g \vec{V}_g \vec{V}_g\right) = -\beta_g \nabla p + \nabla \cdot \bar{\bar{\tau}}_g + S_{mom-g} \\ &\frac{\partial}{\partial t}\left(\beta_l \rho_l \vec{V}_l\right) + \nabla \cdot \left(\beta_l \rho_l \vec{V}_l \vec{V}_l\right) = -\beta_l \nabla p + \nabla \cdot \bar{\bar{\tau}}_l + S_{mom-l} \\ &S_{mom-g} = -\dot{m}\vec{v}_g + Rb_g + Wb_g \\ &S_{mom-l} = \dot{m}\vec{v}_l + \beta_l \rho_l \vec{g} + Rb_l + Wb_l \end{aligned} \tag{4.14}$$

The interactions between the two phases are modeled by adding the source and sink terms due to the condensation and interphase drag to the momentum equations. The resistance force due to the tube bundle is also added as a source term to the momentum equations. The gravity force is only considered for the liquid phase as its effect is almost negligible for the gas phase. In Eq. (4.14), Rb_g and Rb_l are the resistance forces due to the tube bundle for the gas and liquid phases, respectively. The terms Wb_g and Wb_l in Eq. (4.14) represent the interphase drag forces between the gas and liquid phases. The full definition of these drag forces are given in the previous work [32].

Moreover, since the flow in the condenser is turbulent, it is crucial to include the effect of turbulence on the flow and heat transfer in the CFD model. The k-ω SST turbulence

model [39] is selected in this study for this purpose. The turbulence kinetic energy (k) and specific dissipation rate (ω) equations are given as follows:

$$\frac{\partial}{\partial t}\left(\beta_g \rho_g k\right) + \nabla \cdot \left(\beta_g \rho_g k \vec{V}_g\right) = \frac{\partial}{\partial x_j}\left[\beta_g \Gamma_k \frac{\partial k}{\partial x_j}\right] - \beta_g Y_k + \beta_g G_k$$

$$\frac{\partial}{\partial t}\left(\beta_g \rho_g \omega\right) + \nabla \cdot \left(\beta_g \rho_g \omega \vec{V}_g\right) = \frac{\partial}{\partial x_j}\left[\beta_g \Gamma_\omega \frac{\partial \omega}{\partial x_j}\right] - \beta_g Y_\omega + \beta_g G_\omega$$

(4.15)

where Γ_k and Γ_ω represent the effective diffusivity of k and ω, and the terms Y_k and Y_ε represent the dissipation of k and ω due to turbulence, respectively. The local mass fraction of the non-condensable gases (air) is predicted by solving the convection-diffusion equation for the air:

$$\frac{\partial}{\partial t}\left(\beta_g \rho_g \theta\right) + \nabla \cdot \left(\beta_g \rho_g \vec{V}_g \theta\right) = -\nabla \cdot \left(\beta_g \vec{J}\right) + \beta_g S_{diff}$$

(4.16)

where θ is the air mass fraction, J is the diffusion flux of the air in the vapor and S_{diff} is the source term.

Finally, it is important to model the condensation in the condenser. Since it is not computationally feasible to solve the temperature field around each tube in the condenser, a correlation based on the overall energy balance between the shell-side and tube-side is used in this study.

$$\dot{m} L V_L = \frac{T - T_{cw}}{R_{total}} A$$

(4.17)

where L is the latent heat of the condensation, A is the heat transfer area of the tubes located in each computational cell with a volume V, and R_{total} is the total thermal resistance between the shell-side vapor and tube-side cooling water. R_{total} consists of the thermal resistance on the cooling water side (R_{cw}), tube wall resistance (R_{tw}), condensate film resistance (R_c), and resistance due to the non-condensable gas layer (R_a). Both vapour and liquid condensate phases are assumed to be in the saturated state, and the

vapor-air mixture temperature, T, is obtained according to the partial pressure of steam in the gas mixture.

$$R_{total} = R_{cw} + R_{tw} + R_c + R_a \qquad (4.18)$$

The detailed calculation of thermal resistances is provided in the previous work [32].

4.4   Numerical Solution

The optimization design process consists of several coupled processes. For each design, the design parameters are passed to the mesh generation software, ICEMCFD, to create the mesh. The mesh file is then input to the CFD simulation software, ANSYS FLUENT 14.5, to perform the simulation. The output data are then used to obtain the objective functions for the optimization algorithm. The schematic diagram of this process is given in Figure 4-3.

```
┌──────────────────┐
│   Input File     │
│ (Design variables)│
└──────────────────┘
         │
         ▼
┌──────────────────┐
│  Generate Mesh   │
│   (ICEM CFD)     │
└──────────────────┘
         │
         ▼
┌──────────────────┐
│   CFD Solver     │
│ (ANSYS FLUENT 14.5)│
└──────────────────┘
         │
         ▼
┌──────────────────┐
│   Output File    │
│ (Objective Functions)│
└──────────────────┘
```
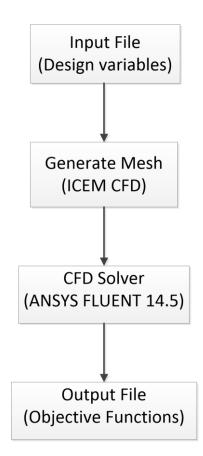
Figure 4-3: Optimization procedure

There are many design variables that can be chosen to optimize the performance of condensers such as the tube configuration, outside diameter, thickness, pitch, material type and other parameters like baffle type, baffle dimensions, etc. However, since the objective of this study is to propose a general method for the condenser optimization, three parameters are chosen to demonstrate the optimization procedure, the tube outside diameter, thickness and pitch. The test case is the shell-and-tube experimental condenser [7], as shown in Figure 4-4. The geometric and operating parameters of this condenser are given in Table 4-1.
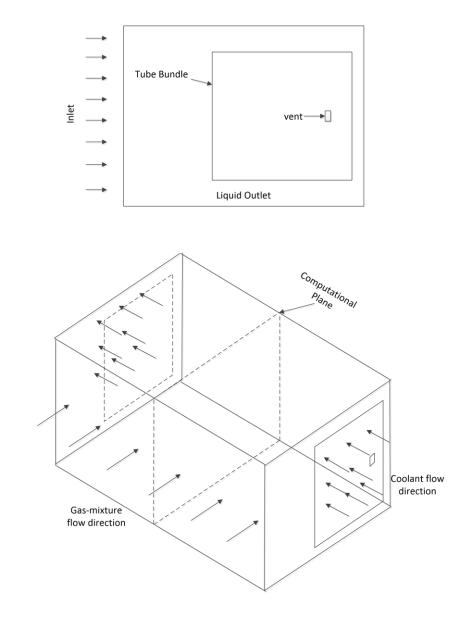
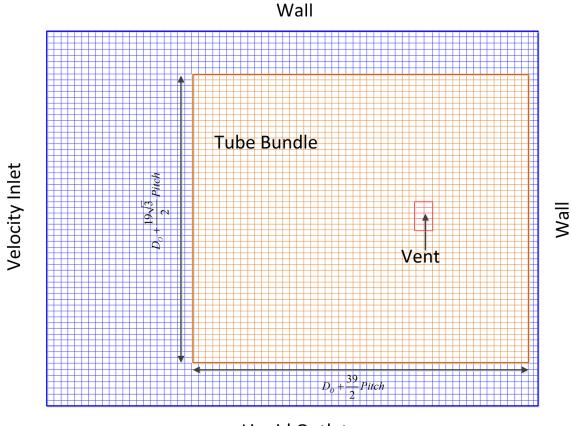**Figure 4-4: Configuration of the experimental condenser**

Table 4-1: Geometric and operating parameters of the condenser used as the base for the design optimization

Geometric parameters	
Number of tubes	400
Condenser length (m)	1.219
Condenser depth (m)	1.02
Condenser height (m)	0.78
Tube outer diameter (mm)	25.4
Tube wall thickness (mm)	1.25
Tube pitch (mm)	34.9
Operating parameters	
Inlet cooling water temperature (C)	17.8
Inlet cooling water velocity (m/s)	1.19
Inlet steam pressure (Pa)	27670
Inlet steam flow rate (kg/s)	2.032
Inlet air flow rate (Kg/s)	2.48e-04

4.4.1   Mesh

The two-dimensional structured mesh is generated for CFD simulations using the ICEM CFD software. Three separate zones are created as shown in Figure 4-5, the tubular region, the vent region and the rest of the condenser where no condensation takes place. The size and dimension of the tubular region are determined based on the tube diameter and pitch, and they are different for different design candidates.

Wall

Velocity Inlet

Tube Bundle

$D_o + \dfrac{19\sqrt{3}}{2} Pitch$

Vent

Wall

$D_o + \dfrac{39}{2} Pitch$

Liquid Outlet

Figure 4-5: Two-dimensional mesh generated for condenser simulations

4.4.2   CFD simulation

The boundary conditions for the condenser walls, outlet, inlet and vent need to be specified.

At the inlet, the velocity is set as uniform based on the inlet mass flow rate. The air mass fraction is also specified at the inlet, which is also uniform. The bottom wall acts as an outlet for the liquid-phase and as a free-slip wall for the gas-phase. The rest of the walls are specified as non-slip walls for both phases. The vent zone is modeled as a mass sink. It is assumed that the amount of vapor that was not condensed around the tubes will leave the domain through the vent along with the air. Also, the air mass fraction at the vent is obtained accordingly. Moreover, the cooling water flow rate is constant for all tubes and its velocity is determined based on the flow rate and the tube diameter, which is different for each design candidate.

All the source terms described in Section 4.3 are implemented into ANSYS FLUENT using User Defined Functions (UDFs). The simulations are performed using a coupled solver for pressure–velocity coupling with very low Courant number (0.1). The first order upwind scheme is chosen for the discretization of the momentum, energy, volume fraction, and turbulent kinetic energy and dissipation rate equations.

4.4.3   Objective functions

There are many objective functions that can be used. To demonstrate the proposed condenser design optimization algorithm, two main objective functions are chosen for this study. The first objective is to increase the condensation rate or minimize the non-condensed steam leaving the domain. The second objective is to minimize the pressure loss from inlet to the vent. These two are considered to be the most important parameters in the condenser design from the thermo-fluids perspective. The objective functions are calculated and reported in an output file from the CFD software, and are used in the optimization algorithm to evaluate the fitness function for each particle.

4.4.4   Optimization setup

The MOTPSO optimization method is used in this study to improve the performance of the selected condenser. The population size of the swarm is taken to be equal to 20 as the CFD simulation of each design configuration is computationally expensive. The size of the external archive, that stores the non-dominated solutions in the optimization process, is chosen to be equal to the swarm size, and the total number of iterations for the optimization algorithm is set as 50. The ranges of the design variables and the detailed setup for the optimization technique are presented in Table 4-2 and Table 4-3 respectively. The design variables' ranges are chosen in a way that the size of tube bundle region is physically realistic.

Table 4-2: Design Variable Range

Design Parameters	Coefficient Range
Tube outer diameter	(15mm, 35mm)
Tube pitch	(25mm, 40mm)
Tube thickness	(0.5mm, 1.5mm)
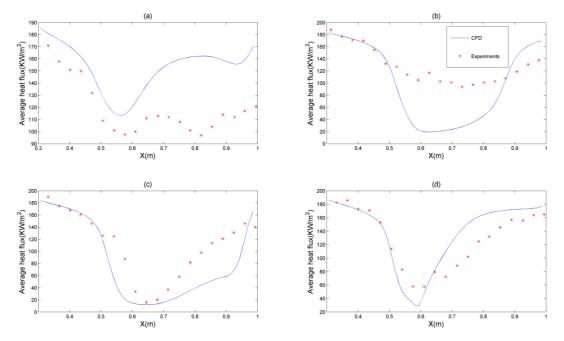
Table 4-3: MOTSPO Parameterization for the condenser optimization
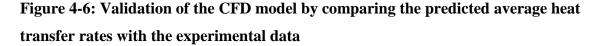
Number of objective functions: 2

Swarm Size: 20

Number of iterations: 50

Mutation polynomial (polynomial distribution index=20)

Archive Size: 30 individuals

Inertia weight (W): (0.9 to 0.4)

Constriction factor (χ): Equations (4.4) and

ϕ_1: Randomly chosen between 1.5 and 2.5

ϕ_2: Randomly chosen between 1.5 and 2.5

ϕ_3: Set to be equal to 1.0

It is important to rule out physically impossible designs from the optimization process. This is accomplished by using numerical constraints in the optimization algorithm. In this analysis, it is assumed that the design in which the distance between the tubes is lower than 5 millimeter is not feasible.

4.5 Results and Discussion

First, it is important to validate the CFD model by comparing the numerical results with the experimental data. The experimental data are taken from the work by Al-Sanea et al. [7], where they reported the average heat transfer rates for tube rows at different locations in the tube bundle. The results are presented in the Figure 4-6.

Figure 4-6: Validation of the CFD model by comparing the predicted average heat transfer rates with the experimental data

The average error calculated from the two-dimensional simulation using the proposed numerical method is 29.65%. A better accuracy can be obtained by using the quasi-three-dimensional or three-dimensional methods that takes into account the effect of the increase in the cooling water temperature in the third direction. As it was reported in the previous works [32, 33], the error can be as low as 11.38% by using the quasi-three-dimensional or three-dimensional method. However, the use of either the quasi-three-

dimensional or three-dimensional approach will significantly increase the computational cost; respectively five and ten times faster than quasi-three-dimensional and three-dimensional model. For the optimization purpose, in which the fitness function is called multiple times in the main program, the two-dimensional modeling can meet the requirements.

The selected condenser parameters are then optimized using the MOTPSO algorithm described in Section 4.2. Because of the multi-objective nature of the optimization process, there is not a unique best design candidate for this problem and a range of non-dominated solutions, which is called Pareto front, are provided by the algorithm shown in Figure 4-7. Each of these design candidates can be a potential condenser configuration based on the specific needs of the designer.
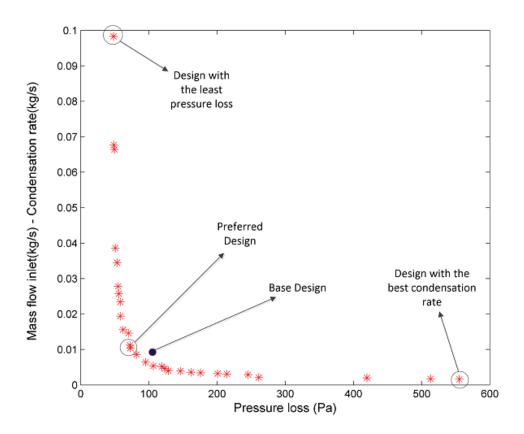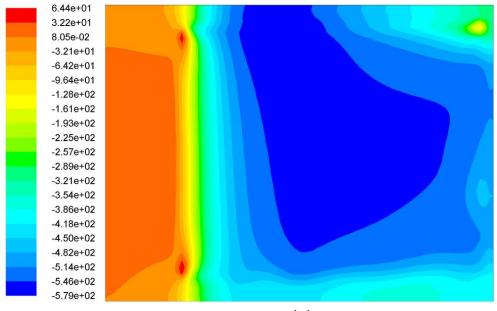

Figure 4-7: Set of non-dominated solution, Pareto front, obtained by the algorithm

The Pareto front provided by the MOTPSO algorithm contains a diverse and distributed set of optimal solutions because of the diversity-preserving capability of the algorithm and the nearest neighbor density estimator quality criterion for the leader selection from the archive. A closer look at the set of the non-dominated solution reveals that the objectives chosen for this optimization study act opposite to each other. In other words, any attempt to improve the performance of the condenser in one of the objectives will worsen its performance in the other. Therefore, the trade-off solution has to be found. To gain a better insight in this regard, two design candidates from the two ends of this spectrum which exhibit minimum values for the particular objectives are demonstrated here. The design parameters and objective functions of the selected designs are reported in Table 4-4: Design parameters and objective functions for the selected designs. The contours of the pressure and condensation rate are given in Figure 4-8 and Figure 4-9, respectively. Moreover, Figure 4-7 demonstrate that the base design is dominated by the Pareto front design solutions.

Table 4-4: Design parameters and objective functions for the selected designs

Designs	Tube outer diameter (mm)	Tube pitch (mm)	Tube thickness (mm)	Condensation rate (kg/s)	Pressure drop (Pa)
Original Design	25.4	34.9	1.25	2.0238	105.581
Lowest pressure loss	15.8	31.3	0.5	1.9334	48.134
Highest condensation rate	34.4	39.8	1.5	2.0304	548.684
Preferred design	21.5	31.0	1.0	2.0214	72.799

Pressure (Pa)

```
6.44e+01
3.22e+01
8.05e-02
-3.21e+01
-6.42e+01
-9.64e+01
-1.28e+02
-1.61e+02
-1.93e+02
-2.25e+02
-2.57e+02
-2.89e+02
-3.21e+02
-3.54e+02
-3.86e+02
-4.18e+02
-4.50e+02
-4.82e+02
-5.14e+02
-5.46e+02
-5.79e+02
```

(a)

Pressure (Pa)

```
5.28e+00
2.60e+00
-7.47e-02
-2.75e+00
-5.43e+00
-8.11e+00
-1.08e+01
-1.35e+01
-1.61e+01
-1.88e+01
-2.15e+01
-2.42e+01
-2.69e+01
-2.95e+01
-3.22e+01
-3.49e+01
-3.76e+01
-4.03e+01
-4.29e+01
-4.56e+01
-4.83e+01
```
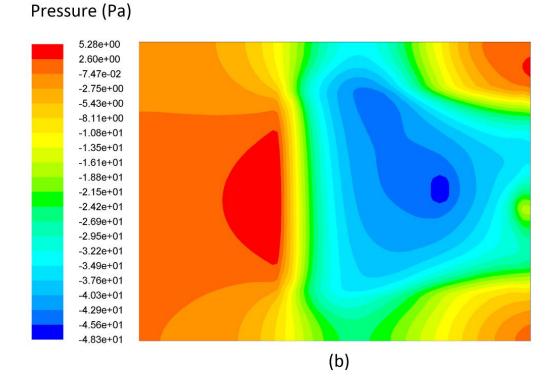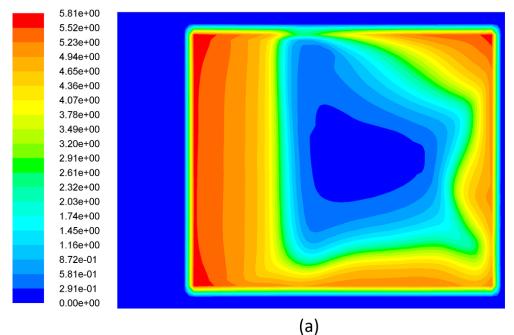
(b)

Figure 4-8: Contours of the pressure for the selected design candidates, (a) highest condensation rate and (b) lowest pressure drop

Condensation Rate (kg/m^3.s)

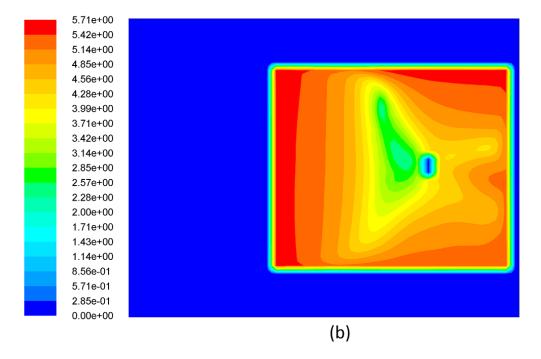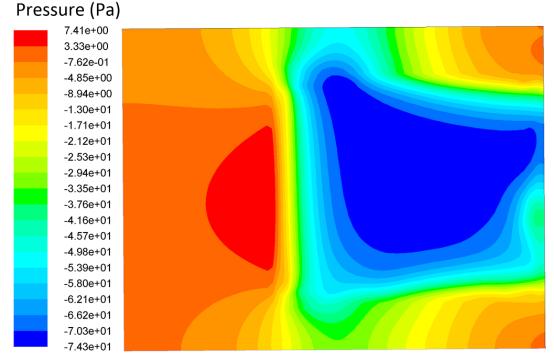
(a)

Condensation Rate (kg/m^3.s)

(b)

Figure 4-9: Contours of the condensation rate for the selected design candidates, (a) highest condensation rate and (b) lowest pressure drop

The design with the highest condensation rate has the tubes with larger diameter and pitch with respect to the design with the lowest pressure loss. The larger tube diameter means more surface area in contact with the shell-side vapor flow. Therefore, the heat and mass transfer rates are increased. Moreover, the tubular region is larger in this case, thus the condensation occurs in a larger portion of the condenser and the available space in the condenser is more effectively used. However, increasing the tube diameter and pitch has some adverse effects on the condenser performance as well. More surface area means more friction and therefore higher pressure loss. Also, by selecting tubes with larger diameter, the coolant flow velocity in the tubes decreases since the coolant mass flow rate stays the same. The lower coolant flow velocity means higher thermal resistance in the tube-side which lowers the heat transfer rate. Consequently, there are many factors affecting the performance of the condenser in both heat transfer and pressure loss perspectives, and a multi-objective design optimization is the only way that can consider all these factors and yield the desired solutions. To select the preferred design, both objective functions were considered to be equally important and a compromised solution was selected as shown in the Pareto front (Figure 4-7). The design parameters and objective functions for the preferred design are shown in Table 4-4 and the condensation rate and pressure contours of the preferred design are illustrated in Figure 4-10.

Pressure (Pa)

(a)

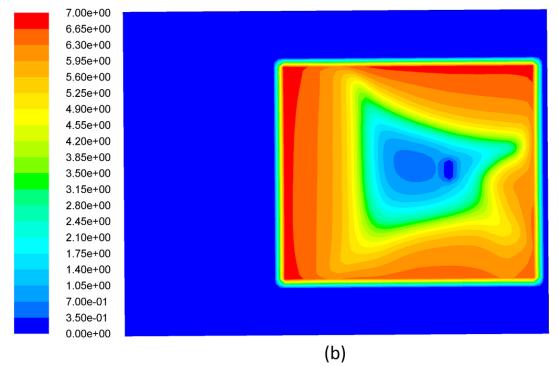Condensation Rate (kg/m^3.s)

(b)

Figure 4-10: Contours of the pressure and condensation rate for the preferred design, (a) pressure and (b) condensation rate

4.6   Conclusions

The Multi-Objective Territorial Particle Swarm Optimization (MOTPSO) algorithm was chosen to perform the design optimization for a small-scale shell and tube steam surface condenser in this study. The tube diameter, pitch and thickness were taken as the design parameters while condensation rate and pressure loss were considered as the objective functions for the proposed algorithm that can be used to improve the design of shell and tube steam surface condensers.

To assess the performance of each design, a two-dimensional Eulerian-Eulerian two-phase CFD model was used to obtain the fluid flow and heat transfer inside the condenser. ANSYS FLUENT solver was chosen to perform the CD simulations.

For the first time, a systematic way of improving the condenser designs using CFD methods and optimization techniques was proposed in this study. The feasibility of the proposed method was validated using a small-scale experimental steam surface condenser with a simple tube bundle configuration. However, the optimization procedure proposed in this study is applicable to larger industrial condensers with more complex tube bundle shapes.

References

[1]   Y. He, W. Tao, B. Deng, X. Li, and Y. Wu, "Numerical simulation and experimental study of flow and heat transfer characteristics of shell side fluid in shell-and-tube heat exchangers," in *Proceedings of Fifth International Conference on Enhanced, Compact and Ultra-Compact Heat Exchangers: Science, Engineering and Technology, Hoboken, NJ, USA*, 2005, pp. 29-42.

[2]   I. S. Ramón and M. P. González, "Numerical study of the performance of a church window tube bundle condenser," *International journal of thermal sciences,* vol. 40, pp. 195-204, 2001.

[3]   H. Zeng, J. a. Meng, and Z. Li, "Numerical study of a power plant condenser tube arrangement," *Applied Thermal Engineering,* vol. 40, pp. 294-303, 2012.

[4]   S. Kakac, H. Liu, and A. Pramuanjaroenkij, *Heat exchangers: selection, rating, and thermal design*: CRC press, 2012.

[5]   M. Prithiviraj and M. J. Andrews, "Three dimensional numerical simulation of shell-and-tube heat exchangers. Part I: foundation and fluid mechanics," *Numerical Heat Transfer, Part A: Applications,* vol. 33, pp. 799-816, 1998.

[6]   B. Davidson and M. Rowe, "Simulation of power plant condenser performance by computational methods: an overview," *Power Condenser Heat Transfer Technology,* pp. 17-49, 1981.

[7]   S. Al-Sanea, N. Rhodes, D. Tatchell, and T. Wilkinson, "A computer model for detailed calculation of the flow in power station condensers," in *Condensers: theory and practice. Symposium*, 1983, pp. 70-88.

[8]   S. Al-Sanea, N. Rhodes, and T. Wilkinson, "Mathematical modelling of two-phase condenser flows," in *Proceedings of the BHRA 2nd International Conference on Multi-Phase Flow, London*, 1985, pp. 169-182.

[9]   T. Rabas and A. Kassem, "The Effect of Equal Shellside Pressure Drops on the Thermal Performance of Single-Pass,'X'-Shell, Steam Condensers," in *23rd ASME-AIChE National Heat Transfer Conference, Denver, Colorado*, 1985.

[10]   J. McNaught and C. Cotchin, "Heat transfer and pressure drop in a shell and tube condenser with plain and low-fin tube bundles," *Chemical engineering research & design,* vol. 67, pp. 127-133, 1989.

[11]   A. Bush, G. Marshall, and T. Wilkinson, "The prediction of steam condensation using a three component solution algorithm," in *Proceedings of the Second International Symposium on Condensers and Condensation, University of Bath, UK*, 1990, pp. 223-234.

[12]   M. R. Malin, "Modelling flow in an experimental marine condenser," *International Communications in Heat and Mass Transfer,* vol. 24, pp. 597-608, 1997.

[13]   R. Roy, V. Gokhale, and M. Ratisher, "A computational model of a power plant steam condenser," *Journal of energy resources technology,* vol. 123, pp. 81-91, 2001.

[14]   M. Prieto, I. Suarez, and E. Montanes, "Analysis of the thermal performance of a church window steam condenser for different operational conditions using three models," *Applied thermal engineering,* vol. 23, pp. 163-178, 2003.

[15]   S. Ormiston, G. Raithby, and L. Carlucci, "Numerical modeling of power station steam condensers—Part 1: Convergence behavior of a finite-volume model," *Numerical Heat Transfer,* vol. 27, pp. 81-102, 1995.

[16]   S. Ormiston, G. Raithby, and L. Carlucci, "Numerical modeling of power station steam condensers—Part 2: Improvement of solution behavior," *Numerical Heat Transfer,* vol. 27, pp. 103-125, 1995.

[17]   H. G. Hu and C. Zhang, "A modified k–ε turbulence model for the simulation of two-phase flow and heat transfer in condensers," *International Journal of Heat and Mass Transfer,* vol. 50, pp. 1641-1648, 2007.

[18]   H. G. Hu and C. Zhang, "Evaluations of closure correlations for the simulation of two-phase flows in condensers," *Heat Transfer Engineering,* vol. 30, pp. 437-451, 2009.

[19]   H. G. Hu and C. Zhang, "A new inundation correlation for the prediction of heat transfer in steam condensers," *Numerical Heat Transfer, Part A: Applications,* vol. 54, pp. 34-46, 2008.

[20]   C. Zhang, "Numerical modeling using a quasi-three-dimensional procedure for large power plant condensers," *Journal of heat transfer,* vol. 116, pp. 180-188, 1994.

[21]   C. Zhang, "Local and overall condensation heat transfer behavior in horizontal tube bundles," *Heat transfer engineering,* vol. 17, pp. 9-30, 1996.

[22]   C. Zhang and A. Bokil, "A quasi-three-dimensional approach to simulate the two-phase fluid flow and heat transfer in condensers," *International journal of heat and mass transfer,* vol. 40, pp. 3537-3546, 1997.

[23]   C. Zhang, A. Sousa, and J. Venart, "The numerical and experimental study of a power plant condenser," *Journal of heat transfer,* vol. 115, pp. 435-445, 1993.

[24] C. Zhang, A. Sousa, and J. Venart, "Numerical simulation of different types of steam surface condensers," *Journal of Energy Resources Technology,* vol. 113, pp. 63-70, 1991.

[25] C. Zhang and Y. Zhang, "A quasi-three-dimensional approach to predict the performance of steam surface condensers," *Journal of energy resources technology,* vol. 115, pp. 213-220, 1993.

[26] C. Zhang and Y. Zhang, "Sensitivity analysis of heat transfer coefficient correlations on the predictions of steam surface condensers," *Heat transfer engineering,* vol. 15, pp. 54-63, 1994.

[27] R. Selbaş, Ö. Kızılkan, and M. Reppich, "A new design approach for shell-and-tube heat exchangers using genetic algorithms from economic point of view," *Chemical Engineering and Processing: Process Intensification,* vol. 45, pp. 268-275, 2006.

[28] J. M. Ponce-Ortega, M. Serna-González, and A. Jiménez-Gutiérrez, "Use of genetic algorithms for the optimal design of shell-and-tube heat exchangers," *Applied Thermal Engineering,* vol. 29, pp. 203-209, 2009.

[29] K. J. Bell, *Delaware method for shell-side design*, Heat Transfer Equipment Design, R.K. Shah et al. eds., CRC Press, pp. 145-166, 1988.

[30] M. Fesanghary, E. Damangir, and I. Soleimani, "Design optimization of shell and tube heat exchangers using global sensitivity analysis and harmony search algorithm," *Applied Thermal Engineering,* vol. 29, pp. 1026-1031, 2009.

[31] V. K. Patel and R. V. Rao, "Design optimization of shell-and-tube heat exchanger using particle swarm optimization technique," *Applied Thermal Engineering,* vol. 30, pp. 1417-1425, 2010.

[32] P. Mirzabeygi and C. Zhang, " Three-Dimensional Numerical Model for the Two-Phase Flow and Heat Transfer in Condensers," Submitted to Int. Jnl. of Heat and Mass Transfer.

[33] P. Mirzabeygi and C. Zhang, " Turbulence modeling for two phase flow and heat transfer in condensers," Submitted to International Journal of Multiphase Flow.

[34] A. Nejat, P. Mirzabeygi, and M. S. Panahi, "Airfoil shape optimization using improved Multiobjective Territorial Particle Swarm algorithm with the objective of improving stall characteristics," *Structural and Multidisciplinary Optimization,* pp. 1-15, 2013.

[35] J. Kennedy and R. Eberhart, "Particle swarm optimization," *Neural Networks, 1995. Proceedings., IEEE International Conference on,* vol. 4, pp. 1942-1948, 1995.

[36]   B. Ostadmohammadi Arani, P. Mirzabeygi, and M. Shariat Panahi, "An improved PSO algorithm with a territorial diversity-preserving scheme and enhanced exploration–exploitation balance," *Swarm and Evolutionary Computation,* vol. 11, pp. 1-15, 2013.

[37]   K. Deb, A. Pratap, S. Agarwal, and T. Meyarivan, "A fast and elitist multiobjective genetic algorithm: NSGA-II," *Evolutionary Computation, IEEE Transactions on,* vol. 6, pp. 182-197, 2002.

[38]   K. Deb, *Multi-objective optimization using evolutionary algorithms* John Wiley & Sons, 2001.

[39]   F. R. Menter, "Two-equation eddy-viscosity turbulence models for engineering applications," *AIAA journal,* vol. 32, pp. 1598-1605, 1994.

Chapter 5

5 Conclusion

A computational fluid dynamics model was proposed in this study to perform the numerical analysis of shell-and-tube steam surface power plant condensers using the commercial software ANSYS FLUENT. The Eulerian-Eulerian, two fluid, multi-phase model was used to simulate the flow and heat transfer for the gas and liquid phases and the interaction between them. The heat and mass transfer between the shell-side flow and the tube-side cooling water flow were modeled using auxiliary correlations implemented using UDFs. The porous media approach was used where the effect of tube bundle was modeled as a distributed resistance against the shell-side flow. The heat transfer deterioration due to the presence of non-condensable gases, mainly air, was considered by solving the species transport equations to obtain the local concentration of non-condensable gases. This concentration then used to model the extra thermal resistance due to the accumulation of non-condensable gases at the gas-liquid interface around the tubes. Furthermore, inundation phenomenon, that is the flooding of the tubes located at the bottom of the tubular region by the condensate falling down from the top, was modeled in this study and the extra thermal resistance due to the increased condensate thickness around the bottom tubes was accounted for.

For the first time, both three-dimensional and quasi-three-dimensional approaches were implemented to solve the flow and heat transfer inside a small-scale experimental condenser and a large-scale industrial condenser. The numerical method was shown to be successful in modeling the condensation inside both the small and large-scale condensers. The industrial condensers usually have more complex and irregular tube bundle shape with thousands of tubes that makes the problem extremely more challenging to analyze. Moreover, there are several tube support sheets that carry the weight of the tubes and restrict the flow in the third direction which adds to the difficulty of the problem.

The mixture of steam and non-condensable gases is turbulent. Therefore, it is crucial to consider the turbulence effects on the shell-side gas-mixture flow. A comparative

analysis was conducted to compare the performance of various turbulence models on predicting heat and mass transfer inside the condenser. Amongst different turbulence models, *k-ω SST* model was the most successful one. Moreover, to model the effects of the porous medium and the liquid condensate droplets on the primary phase turbulent kinetic energy and dissipation rates, the modified *k-ε* and RNG *k-ε* turbulence models were proposed in this research. They significantly improved the accuracy of the numerical results with respect to the original turbulence models.

Finally, a multi-objective optimization technique was used to propose a systematic way to improve the performance of the shell-and-tube condensers. Several design parameters were chosen and the MOTPSO optimization algorithm was used to find the set of improved solutions among the design space. The two-dimensional version of the proposed numerical model was used to assess the performance of each design candidate. The outcome of the design optimization was a set of solutions with improved the condensation rate and pressure drop that provides the designer a range of desired characteristics to choose from. This study provides the structure for the future design optimization of condensers with more complex tube bundle configurations.

Curriculum Vitae

Name:	Pooya Mirzabeygi
Post-secondary Education and Degrees:	University of Tehran Tehran, Iran 2007-2012 B.Sc. The University of Western Ontario London, Ontario, Canada 2012-2014 M.Sc.
Honours and Awards:	Graduate Research Scholarship 2012-2014
Related Work Experience	Research Assistant The University of Western Ontario 2012-2014 Teaching Assistant The University of Western Ontario 2012-2014

Publications:
Mirzabeygi, P., Zhang, C. (2014). Computational Fluid Dynamic Analysis of two phase flow and Heat Transfer in Condensers, CSME International Congress 2014, Toronto, Ontario, Canada, June 1-4.

Mirzabeygi, P., Zhang, C. (2014). Computational Fluid Dynamics Modeling of Laminar Film Condensation on a Horizontal Tube, 22nd Annual Conference of the CFD Society of Canada. Toronto, Ontario, Canada, June 1-4.

Nejat, A., Mirzabeygi, P., Shariat Panahi, M. (2013). Airfoil shape optimization using improved Multiobjective Territorial Particle Swarm algorithm with the objective of improving stall characteristics. Structural and Multidisciplinary Optimization, 49, 1-15.

Arani, B., Mirzabeygi, P., Shariat Panahi, M. (2013). An Improved PSO Algorithm with a Territorial Diversity-Preserving Scheme and Enhanced Exploration-Exploitation balance, Swarm and Evolutionary Computation, 11, 1-15.

Nejat, A., Mirzabeygi, P., Shariat Panahi, M. (2012). Aerodynamic Shape Optimization Using Improved Territorial Particle Swarm Algorithm, ASME 2012 International Mechanical Engineering Congress and Exposition, 1, 509-517.

Nejat, A., Mirzabeygi, P., Shariat Panahi, M., Mirzakhalili, E. (2012). Heat Transfer Enhancement Across A Pair Of Confined Cylinders Using Improved Particle Swarm Optimization Algorithm, ASME 2012 International Mechanical Engineering Congress and Exposition, 7, 577-585.